ASPHALT OXIDATION KINETICS AND PAVEMENT OXIDATION MODELING

A Dissertation

by

XIN JIN

Submitted to the Office of Graduate Studies of
Texas A&M University
in partial fulfillment of the requirements for the degree of

DOCTOR OF PHILOSOPHY

May 2012

Major Subject: Chemical Engineering

Asphalt Oxidation Kinetics and Pavement Oxidation Modeling

ASPHALT OXIDATION KINETICS AND PAVEMENT OXIDATION MODELING

A Dissertation

by

XIN JIN

Submitted to the Office of Graduate Studies of
Texas A&M University
in partial fulfillment of the requirements for the degree of

DOCTOR OF PHILOSOPHY

Approved by:

Chair of Committee,	Charles J. Glover
Committee Members,	Amy Epps Martin
	M. Sam Mannan
	Victor M. Ugaz
Head of Department,	Charles J. Glover

May 2012

Major Subject: Chemical Engineering

ABSTRACT

Asphalt Oxidation Kinetics and Pavement Oxidation Modeling. (May 2012)

Xin Jin, B.E., Zhejiang University;

M.S., Texas A&M University

Chair of Advisory Committee: Dr. Charles J. Glover

Most paved roads in the United States are surfaced with asphalt. These asphalt pavements suffer from fatigue cracking and thermal cracking, aggravated by the oxidation and hardening of asphalt. This negative impact of asphalt oxidation on pavement performance has not been considered adequately in pavement design. Part of the reason is that the process of asphalt oxidation in pavement is not well understood.

This work focused on understanding the asphalt oxidation kinetics and on developing pavement oxidation model that predicts asphalt oxidation and hardening in pavement under environmental conditions.

A number of asphalts were studied in laboratory condition. Based on kinetics data, a fast-rate – constant-rate asphalt oxidation kinetics model was developed to describe the early nonlinear fast-rate aging period and the later constant-rate period of asphalt oxidation. Furthermore, reaction kinetics parameters for the fast-rate and constant-rate reactions were empirically correlated, leading to a simplified model. And the experimental effort and time to obtain these kinetics parameters were significantly reduced. Furthermore, to investigate the mechanism of asphalt oxidation, two

antioxidants were studied on their effectiveness. Asphalt oxidation was not significantly affected. It was found that evaluation of antioxidant effectiveness based on viscosity only is not reliable.

The asphalt oxidation kinetics model was incorporated into the pavement oxidation model that predicts asphalt oxidation in pavement. The pavement oxidation model mimics the oxidation process of asphalt in real mixture at pavement temperatures. A new parameter, diffusion depth, defined the oxygen diffusion region in the mastic. A field calibration factor accounted for the factors not considered in the model such as the effect of small aggregate particles on oxygen diffusion. Carbonyl area and viscosity of binders recovered from field cores of three pavements in Texas were measured and were used for model calibration and validation. Results demonstrated that the proposed model estimates carbonyl growth over time in pavement, layer-by-layer, quite well.

Finally, this work can be useful for incorporating asphalt oxidation into a pavement design method that can predict pavement performance with time and for making strategic decisions such as optimal time for maintenance treatments.

ACKNOWLEDGEMENTS

I would like to thank my committee chair, Dr. Charles J. Glover, and my committee members, Dr. Amy Epps Martin, Dr. Victor M. Ugaz, Dr. M. Sam Mannan, for their guidance and support throughout the course of this research.

Thanks also go to my colleagues, Yuanchen Cui, Guanlan Liu, Rongbin Han, Jim Lawrence, Edith Arambula, Padigala Meghana, and Arif Chowdhury. Without them, this work would not be possible.

Finally, thanks to my parents for their encouragement and to my wife for her patience, love, and professional help on statistics.

TABLE OF CONTENTS

CHAPTER Page

LIST OF FIGURES

FIGURE Page

LIST OF TABLES

CHAPTER I

INTRODUCTION

Asphalt concrete pavements comprise about 94 percent of paved roads in the United States, covering about 1.9 million miles. These asphalt pavements are subject to three major distresses: rutting at high temperatures, fatigue cracking under repeated traffic loading, and thermal cracking at low temperatures. As pavements deteriorate over time, maintenance costs the government billions of dollars each year. To reduce this cost, a pavement must be well designed such that it has good resistance to distresses. As part of pavement design, the mixture design of the asphalt surface course is extremely important. The Mechanistic-Empirical Pavement Design Guide (MEPDG) was developed in National Cooperative Highway Research Program (NCHRP) project 1-37A, to aid engineers in designing pavements with adequate performance.

The goal of the NCHRP project 1-37A was to develop a design procedure that takes climate and traffic data as inputs, uses material properties as model parameters, and predicts pavement performance through the modeling of pavement responses to loads. Upon completion of the project, the MEPDG in the form of a software program was developed for user evaluation along with a database of climate data. Although the MEPDG provides a tool for evaluating pavement performance and the quality of pavement design, the effect of asphalt oxidation on pavement performance is not well

---

This dissertation follows the style of *Petroleum Science and Technology*.

considered. It assumed that asphalt does not oxidize beyond the top 25-mm layer and asphalt oxidation has no fundamental impact on fatigue resistance of the pavement. However, both laboratory and field data showed that asphalt oxidation must be incorporated into the pavement design because of its tremendous impact on asphalt properties, mixture properties, and consequently pavement durability and performance (Glover et al., 2005). As asphalt oxidizes, it hardens and loses ductility. Correspondingly, the asphalt pavement becomes less and less able to release the stress build-up in the materials and thus cracks occur. Without considering the effect of asphalt oxidation on pavement performance, the predicted results of the MEPDG can be misleading.

To incorporate asphalt oxidation into pavement design for pavement performance prediction purposes, it is critical to understand asphalt oxidation kinetics as a function of temperature because pavement temperature changes with time and depth. It is also worthwhile to investigate the underlying oxidation mechanism and to examine the possible reaction pathways. Furthermore, a pavement oxidation model is needed to predict asphalt oxidation in pavements. Such a model should utilize the oxidation kinetics of asphalt and consider real pavement situations such as pavement temperature and air voids in the mixture. The predicted results, if accurate enough, can be incorporated into the pavement design to predict pavement performance.

Objectives

The objectives of this research are threefold:

1. To obtain asphalt oxidation kinetics data during both an early fast-rate period and a later constant-rate period, and to develop an asphalt oxidation kinetics model that predicts asphalt oxidation at atmospheric air pressure and various temperatures.

2. To study the possible mechanism of asphalt oxidation, especially during the early fast-rate period by evaluating the effectiveness of antioxidants.

3. To improve and validate the pavement oxidation model that utilizes asphalt oxidation kinetics to predict asphalt oxidation in pavement after construction.

Literature Review

The literature review is presented for these objectives subsequently.

Asphalt Oxidation and Hardening

The study of asphalt oxidation dates back to the 1950's. Van Oort (1956) studied the oxygen absorption and logarithmic viscosity change with aging time on several binders aged at room temperature and atmospheric air pressure. Both properties showed a fast increase during an early time period with a declining rate, and then reached a constant rate at a later time. Herrington (1998) observed a similar trend in logarithmic viscosity of two asphalts aged at three constant temperatures (323, 333, and 343 K) and 2 MPa (about 20 atm) air pressure. He proposed a model, which superimposed a first order reaction and a zero order reaction, to match the early fast-rate period and constant-rate period behavior, and obtained reaction constants for both periods.

Most previous work on asphalt oxidation (Liu et al., 1996; Domke et al., 1999; Glover et al., 2005) focused on constant-rate kinetics of binder oxidation. Liu et al.

(1996) found that oxygen uptake is linearly correlated to carbonyl growth. And the carbonyl formation rate during the constant-rate period is:

$$r = AP^{\alpha}e^{-E_a/RT} \quad (1.1)$$

where A is the frequency factor, P is oxygen pressure, α is the reaction order with respect to oxygen pressure, E_a is the activation energy, R is the gas constant, and T is the absolute temperature (K). The rate of carbonyl formation, or the rate of oxidation, is dependent on oxygen partial pressure, temperature, and activation energy. Binders from different sources have different activation energies and reaction orders, and thus different aging rates at the same temperature.

Some studies characterized the fast-rate period as an initial jump, which is the intercept of a constant-rate reaction line of carbonyl area formation (Liu et al., 1996; Domke et al., 1999; Glover et al., 2005). Liu et al. (1996), based on a study of 15 asphalts, concluded that while the initial jump is not a function of temperature, it is a function of oxygen pressure. However, the kinetics of asphalt oxidation during this fast-rate period were not studied.

Jin (2009) proposed an asphalt oxidation kinetics model in terms of carbonyl formation based on aging data of two asphalt binders at five temperatures and air pressure. The model assumed that carbonyl area is formed through two parallel reactions, one first order reaction and one zero order reaction with respect to some unknown species in asphalt. This model fits experimental data very well and can be readily used for prediction purposes. Therefore, aging studies of other asphalts will be worthwhile for validating the model and expanding the database of kinetics parameters.

Asphalt Oxidation Mechanism

The asphalt oxidation mechanisms cited in the literature generally fall into three groups: the free radical chain reaction (FRCR) mechanism (including recent studies on antioxidants), Beaver's electron transfer initiated oxidation (ETIO) mechanism (to explain diesel fuel sedimentation), and Herrington's research on oxidation of asphalt components.

The free radical chain reaction (FRCR) mechanism was proposed and supported by several research studies. Knotnerus (1972) detected by experiment the presence of stable free radicals in asphalt-solvent solutions and reported various antioxidants that worked as free radical scavengers. Martin (1966) and Petersen (2009) had also proposed free radical chain reactions and suggested the benzyl carbons as the main participating reactant in asphalt. However, van Gooswilligen et al. (1985) concluded that asphalt oxidation is not a free radical reaction because the rate was not affected by adding free radical initiators.

The second reaction pathway, electron transfer initiated oxidation (ETIO), was originally proposed for sediment formation in diesel fuel (Beaver et al., 1991). The major oxidative reactants studied were pyrroles and indoles. In the ETIO mechanism, the triplet oxygen reacts with electron-rich compounds (e.g. pyrroles) to form a charge-transfer complex. The oxygen molecule in the charge-transfer complex then attracts one electron from the electron-rich compound, forming the electron-transfer complex. This complex then rapidly forms peroxide that leads to oxidation products and sediments. King applied the ETIO mechanism later to asphalt oxidation, and proposed a catalyzed

oxycyclic oxidation mechanism (King, 1993). This mechanism is uncontrollable and is not affected by antioxidants. King's theory rationalized the formation of various oxidation products including ketones from benzylic carbon. Due to the presence of pyrrolic types and benzylic carbon in asphalt, this reaction pathway may also be important in binder oxidation.

Herrington (2004) proposed inhibited free radical autoxidation for asphaltenes in solution. He suggested that the oxidation was inhibited by natural occurring free radical inhibitors. This is in agreement with the conclusion of van Gooswilligen et al. (1985).

All three proposed mechanisms have difficulty explaining the "fast-rate plus constant-rate" model of binder oxidation. The reactions during the fast-rate period and the constant-rate period might follow different reaction pathways. One way to probe this possibility is by examining the effect of antioxidants on kinetics.

Most researchers address the effectiveness of antioxidants based on comparison of rheological properties, typically viscosity (Apeagyei, 2006; Williams et al., 2008). However, antioxidants might change the binder hardening in two aspects: 1) slow down oxidation rates and 2) make the binder softer or harder by changing the binder composition and compatibility. Therefore, for the purposes of studying the mechanism, those two aspects should be studied separately.

Furthermore, while the oxidation of asphalt goes through an early fast-rate period then a constant-rate period, most antioxidant studies evaluated binders after short-term and long-term laboratory aging methods without considering these two different periods. It is possible that antioxidants only work during one of these two periods while the other

is not affected. Therefore, binders should be aged and sampled during both the fast-rate and constant-rate periods, to provide a chronological view of the function of antioxidants.

Pavement Oxidation Modeling

Of great interest are how fast and to what extent asphalt ages in pavement. Instead of drilling cores from pavements and measuring properties, modeling pavement oxidation with field calibration is definitely more economical. A pavement oxidation model was first developed by Lunsford (1994) and later improved by Prapaitrakul (2009) and Han (2011c). This improved model was developed to predict asphalt oxidation rates (carbonyl content increase per year) in pavements and results were compared with field measurements.

The pavement oxidation model is developed to represent the oxygen transport and reaction process in pavements. The mixture consists of aggregate particles and asphalt as the binder. Due to design requirements, a certain amount of air voids is left inside the mixture. Oxygen existing in irregular interconnected air void channels diffuses from these channels into asphalt films coating aggregate particles, driven by an oxygen partial pressure gradient. At the same time, oxygen reacts with asphalts, making the asphalt film stiffer and less permeable to oxygen (i.e. smaller oxygen diffusion coefficient). Both reaction and diffusion processes are affected by temperature. The asphalt pavement layer is usually 50 to 76 mm thick and the temperatures are different with depth, and vary from hour to hour, from day to night, and from season to season.

For this purpose a pavement temperature model was developed to calculate temperature in pavements as a function of time and depth (Han et al., 2011a).

The model was developed in a cylindrical system, assuming all air void channels are cylindrical and uniformly allocated. Air voids were imaged using X-ray Computed Tomography (CT), and its size (or radius) distribution analyzed. The total number of air voids determines the distance of two air void channels, and the size of each air void channel determines the distance of oxygen diffusion in the asphalt film.

The governing equation for this model is:

$$\frac{\partial P}{\partial t} = \frac{1}{r}\frac{\partial}{\partial r}\left(rD_O\frac{\partial P}{\partial r}\right) - \frac{c}{h}r_{CA} \tag{1.2}$$

where t is time (hour), r is position in cylindrical coordinates (meter), P is oxygen partial pressure (atm), D_O is oxygen diffusivity in asphalt (m^2/hour), c is a conversion factor that converts rate of carbonyl formation to rate of oxygen consumption (mol O_2/[mL asphalt]/CA), h is the solubility constant of oxygen in asphalt (mol O_2/[mL asphalt]/[atm oxygen pressure in gas phase]), and r_{CA} is the rate of carbonyl formation (CA/hour).

Using this model, Han (2011c) compared model calculated pavement oxidation rates with measured rates (CA per year) for six pavement sites, and results were quite encouraging. However, several deficiencies in this model are observed. First, the most important factor of asphalt oxidation in pavement is not the amount or volume of air voids, but rather the surface area of asphalt exposed to air. Converting irregular air void channels to cylindrical channels based on equal volume inevitably reduced the exposed surface area of asphalt. This questions the validity of the cylindrical system assumption. Second, it is never clear how much asphalt really gets aged in the model, because there

is no boundary for the asphalt film, only the distance between air void channels. The amount of asphalt in pavement, which subsequently affects the diffusion depth of oxygen, must be considered as a parameter in the model. Third, as asphalt in pavement is more aged, it becomes less permeable to oxygen, and the oxidation rate should decrease over the years. Therefore, it is not accurate to describe pavement oxidation using a single oxidation rate (e.g. the increase of CA per year), but rather specifying CA as a function of time is more appropriate. Finally, a field calibration factor is needed to account for other factors that are not yet considered in this model, for example, the effect of aggregate particles on hindering oxygen diffusion.

Dissertation Outline

This dissertation is outlined as follows. Chapter II develops a fast-rate – constant-rate asphalt oxidation model that covers both an early fast-rate aging period and a later constant-rate period. Chapter III investigates possible mechanisms of asphalt oxidation. Chapter IV improves the pavement oxidation model by incorporating the fast-rate – constant-rate asphalt oxidation model and other important concepts and validates the model using field data. Finally, the important research findings are summarized and future work is suggested in Chapter V.

CHAPTER II

FAST-RATE – CONSTANT-RATE OXIDATION KINETICS MODEL FOR ASPHALT BINDERS*

Introduction

The significant impact of asphalt oxidative aging on asphalt hardening and pavement performance is well recognized (Branthaver et al., 1993; Walubita et al., 2006; Hajj et al., 2005; Al-Azri et al., 2006). Many research projects have been conducted and others are under way to address relevant issues such as the effect of oxidative aging on fatigue and on thermal cracking and moisture susceptibility (Glover et al., 2009; Cortez et al., 2009). Changes to asphalt chemical and rheological properties due to oxidative aging are among the most important topics.

Asphalts typically oxidize in two stages, a nonlinear fast-rate period and a linear constant-rate period (Van Oort, 1956; Liu et al, 1996; Petersen et al., 1998; Petersen et al., 2009). For asphalts aged in thin films in the laboratory at temperatures approximating field conditions and provided diffusion resistance is minimized by oxidizing sufficiently thin films, a constant-rate oxidation period has been observed to an extensive aging level that goes well beyond field aging levels that exist at the end of a mixture's serviceable life (Liu et al., 1996). Most previous work focused on

---

*Parts of this chapter are reprinted with permission from "Fast-Rate–Constant-Rate Oxidation Kinetics Model for Asphalt Binders" by Xin Jin et al., 2011. *Ind. Eng. Chem. Res.* Vol. 50, 13373-13379, Copyright 2011 by American Chemical Society.

constant-rate kinetics of binder oxidation (Liu et al., 1996; Domke et al., 1999; Glover et al., 2005) because the duration of the fast-rate period was assumed to be relatively short and with a smaller impact on long-term pavement performance. However, field data showed that the fast-rate period was not passed during hot-mix production and construction, and the amount of aging during the fast-rate period after construction may be significant, equivalent to about four years of constant-rate aging in the field in Texas (Glover et al., 2005). This phenomenon was even more obvious for pavements in cold climate region such as Minnesota. Evaluation of binder aging without considering the fast-rate period potentially introduces a large amount of error.

Fast-rate oxidation of binder has long been noted in laboratory aging experiments. Van Oort (1956) studied the oxygen absorption and viscosity change with time of several binders aging at room temperature and atmospheric pressure. Both oxygen absorption and viscosity changes showed a fast increase at early times, and then the rates of change decreased to slower, constant rates at later times. Herrington (1998) aged several types of binders at constant temperatures (323, 333 and 343 K) and 2 MPa air pressure. Viscosities at 333 K were measured at different aging times. Herrington proposed a model in logarithmic viscosity of two reactions occurring in parallel:

$$P = M(1 - e^{-k_2 t}) + kt \tag{2.1}$$

where P is the change of logarithmic viscosity, k and k_2 are reaction constants for the zero order reaction and first order reaction, respectively, M is the maximum or long-term change in log viscosity due to the first reaction. Analysis of the temperature dependence

of the reaction constants k and k_2 for two binders (S180 and I180) suggests that both reaction constants follow Arrhenius kinetics.

Martin et al. (1990) found that changes in logarithmic viscosity show a linear relationship with changes in carbonyl area during the constant-rate aging period. This correlation between carbonyl area and viscosity is termed "Hardening Susceptibility." It relates the formation of carbonyl compound to viscosity, thus relates carbonyl area to performance. If the same relationship holds for the fast-rate aging period, then a similar two-reaction model can be developed in terms of carbonyl area.

Such a model is needed for predicting binder oxidation in pavement as a function of depth (Prapaitrakul et al., 2009) and may be incorporated into pavement design to reflect the impact of aging on pavement performance. Extensive laboratory studies on constant-rate binder aging showed that each type of binder has different aging and hardening kinetics parameters (Lau et al., 1992; Liu et al., 1996). An oxidation kinetics model that includes both fast-rate and constant-rate parameters for individual asphalts will provide more accurate and fundamentally sound design information.

In this chapter, twenty asphalt binders were studied for oxidation kinetics during both fast-rate and constant-rate periods. Kinetics data were analyzed and a fast-rate – constant-rate oxidation kinetics model was developed. More interestingly, empirical correlations between kinetics parameters were found.

Objectives

The objectives of this study were 1) to propose and validate a fast-rate, constant-rate oxidation kinetics model for asphalt binders at temperatures approximating field

conditions for the purpose of pavement oxidation modeling, 2) to investigate the change of the low shear rate limiting complex dynamic viscosity with oxidative aging for both the fast-rate and constant-rate periods, 3) to analyze the sensitivity of model parameters to experimental uncertainties, and 4) to investigate possible correlations between fast-rate and constant-rate kinetics parameters. A successful search for such correlations would be very useful in reducing experimental time and effort, and potentially could provide useful information about the reaction mechanisms. The kinetics parameters for both the fast-rate and constant-rate regimes were determined in terms of changes in the level of oxidation (represented by FTIR carbonyl measurements) rather than changes in rheology in order to provide a better understanding of the reaction chemistry and possible commonalities among different asphalts in relationships between these two kinetics regimes. To base the kinetics analysis on a bottom-line performance measure, such as binder rheology or even mixture durability, while it might seem advantageous from an applications perspective, would totally obscure such commonalities in inter-asphalt kinetics relationships because of the highly material dependent correlations between carbonyl growth and changes in either binder or mixture rheology.

Experimental Methods

Materials

Twenty asphalt binders were selected for the oxidation kinetics study, including ten unmodified binders and ten polymer-modified binders, shown in Table 1. Binders from the same manufacturer did not necessarily share the same base binder, because

some of them were obtained at different years and probably from different crude sources. All binder grades follow the Superpave performance grading (PG) system (Asphalt Institute, 1994). Taking PG 64-22 as an example, 64 (°C) and -22 (°C) are the high and low temperatures at which the binder meets performance requirements. Table 2.1 also shows the carbonyl area and the low shear rate limiting viscosity (measured at 333K) of unaged tank asphalt. These properties were measured as indicated in Section 3.3.

Table 2.1

Twenty Asphalt Binders Selected for Kinetics Study

Manufacturer	**Grade**	**CA_{tank}**	**Viscosity (Pa•s) (@333K)**
Alon	PG 64-22	0.587	482
Alon	PG 70-22 (SBS)	0.474	1828
Alon	PG 76-22 (SBS)	0.563	2225
Lion	PG 64-22	0.542	517
Martin	PG 64-22	0.581	472
Martin	PG 70-22 (SBS)	0.584	2594
SEM	PG 64-22	0.548	362
SEM	PG 70-22 (SBS)	0.503	984
SEM	PG 70-28 (SBS)	0.526	2769
SEM	PG 76-22 (SBS)	0.556	6347
Valero-C	PG 64-22	0.432	504
Valero-C	PG 70-22 (SBS)	0.535	2221
Valero-C	PG 76-22 (SBS)	0.515	8757
Valero-H	PG 76-22 (SBS)	0.555	4948
Valero-O	PG 64-22	0.539	500
NuStar	PG 67-22	0.620	-
NuStar	PG 76-22	0.650	-
Valero-B	PG 64-16	0.770	-
AAD-1	-	0.794	-
AAM-1	-	0.463	-

Aging Procedure

Asphalt binders were prepared in aluminum trays of 4 cm by 7 cm. About 2.4 grams of asphalt were used in each tray to form a film of about 0.8 mm. Such a film thickness minimizes the effect of oxygen diffusion while also providing enough sample for testing. Sample trays were held in racks with a capacity of about 60 trays. These racks were contained in pressure oxygen vessels (POV) at atmospheric air pressure and three to five elevated temperatures (between 333 and 373 K).

These conditions were selected to match actual aging conditions of asphalts in pavements. All temperatures were below 373 K because a different balance of reactions takes place above 373 K (Pfeiffer, 1950). It is expected that kinetics information thus obtained can be used in pavement oxidation modeling at environmental conditions for pavement performance prediction purposes. As such, a model first would estimate binder oxidation; then separate determinations of the impact of oxidation on binder rheology and mixture performance would be applied to predict actual performance.

The POVs were submerged in triethylene glycol (TEG) and water baths with temperatures controlled nominally at 333, 343, 353, 362, and 371 K. The liquid in the baths was continuously stirred to minimize the temperature gradient in the POVs. In addition, the POVs were purged with preheated atmospheric air to maintain atmospheric oxygen concentration. The actual aging temperatures inside the vessels were measured continuously using thermocouples, and the fluctuations were within 0.6 K of the median temperatures. As binders aged, two to three replicate samples were collected at each scheduled time point in accordance with Table 2.2.

Table 2.2

Sampling Times for Asphalt at Different Aging Temperatures

Nominal Aging Temperature (K)	Aging Time (Days)
333	2, 5, 10, 20, 30, 45, 60, 90
343 and 353	1, 3, 5, 7, 10, 20, 30, 40, 50
362 and 371	1, 2, 4, 6, 10, 15, 20, 25, 30

Materials Characterization

Two analytical techniques were used to characterize the unaged and aged binders. Before each measurement, samples on the trays were melted and mixed to obtain a bulk reading. A Thermo Scientific Nicolet 6700 Fourier-Transform Infrared (FTIR) spectrometer measured the carbonyl area using the attenuated total reflectance (ATR) method (effective path length is about 4 micron). Carbonyl area is defined as the integrated peak area from 1820-1650 cm^{-1}, measured in arbitrary units, a.u., as a surrogate of asphalt oxidation level (Jemison et al., 1992). A Carri-Med CSL 500 controlled stress rheometer measured the low shear rate limiting complex viscosity (LSV), for evaluation of asphalt hardening. The fixture is 25 mm in diameter and the gap is 500 microns. The LSV is obtained by a frequency sweep from 0.1 rad/s to 100 rad/s at 333 K (Ruan et al.; 2003). For stiff binders, of which LSV was not obtained at 333 K, an additional frequency sweep was performed at a higher temperature (e.g. 353 K) and time-temperature superposition (TTSP) was used to construct a master curve which gave the LSV (Anderson et al., 1994). For heavily aged polymer modified binders, LSV data

were not obtained due to the difficulties of reaching a plateau even with TTSP. All LSV data reported herein were obtained at stress levels less than 2×10^4 Pa•s, a level reported to be within the linear viscoelastic region (Petersen et al., 1983).

Results and Discussion

Analysis of Carbonyl Area Data

Carbonyl area (CA) data were measured for all 20 binders aged to different times at different temperatures. Both neat and modified binders showed qualitatively similar kinetics results; data for one representative binder Alon PG 64-22 are presented in the following discussion. Figure 2.1 shows the CA growth with time at five aging temperatures. Dashed lines are model calculations that will be explained below. The actual measured temperatures in the aging vessels are shown in Figure 2.1, instead of the set points for the temperature baths. Of course, aging rates are faster at higher temperatures for both the non-linear fast-rate period and linear constant-rate period.

The carbonyl area formation with time at each temperature is modeled according to the following equations:

$$CA = CA_t + M(1 - e^{-k_f t}) + k_c t \tag{2.2}$$

$$k_f = A_f e^{-E_{af}/RT} \tag{2.3}$$

$$k_c = A_c e^{-E_{ac}/RT} \tag{2.4}$$

where $M = (CA_0 - CA_{\text{tank}})$, CA_{tank} is the carbonyl area of the unaged tank asphalt, CA_0 is the intercept of the constant-rate line, k_f and k_c are two reaction constants that are temperature dependent according to the Arrhenius eqs 2.3 and 2.4.

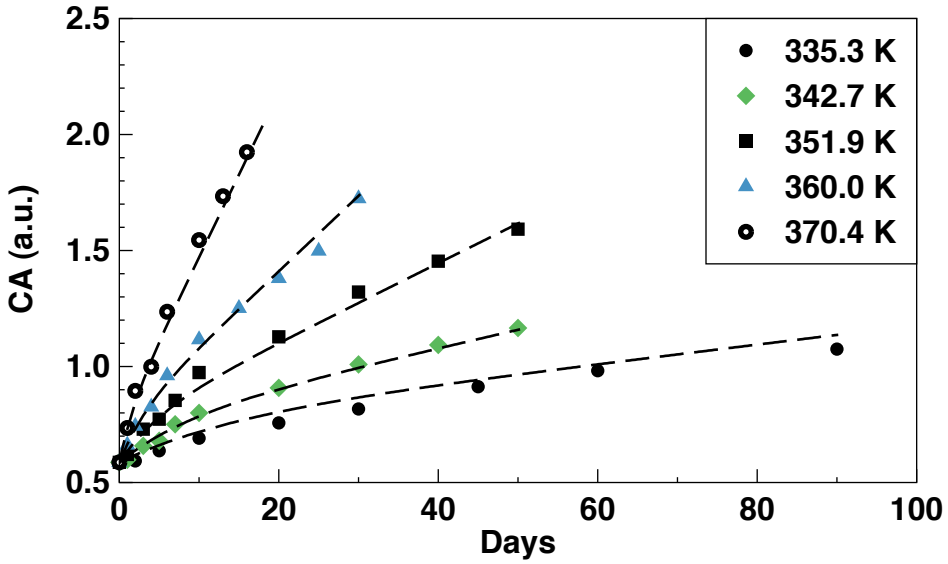

Figure 2.1. CA growth of Alon PG64-22 at five temperatures in air. (Data: Symbols, Model Calculations: Dashed Lines)

Note that *M* is not temperature dependent, but is asphalt source dependent and oxygen partial pressure dependent (Liu et al., 1996; Domke et al., 2000). Domke et al. (2000) found that *M* values (at the same oxygen partial pressure) for different asphalts can be related to its compositional parameter, heptane asphaltenes and pentane asphaltenes ratio (C7/C5), with *M* values decreasing with increasing C7/C5 ratio. This suggests a method for obtaining *M* value from compositional analysis without time-consuming aging experiments.

The three terms in eq 2.2 incorporate the three elements important to the aging process. The first term is the initial carbonyl area for the unaged tank asphalt, the aging starting point. The second term characterizes the fast-rate aging process that follows a first-order reaction that terminates on the depletion of reactants. Three model parameters M (or equivalently $CA_0 - CA_{\text{tank}}$), A_f, and E_{af} are associated with this first-order reaction. These parameters also determine the transition from fast-rate period to constant-rate period, a transition that, in principle, occurs over an infinitely long period. However, practically, the first-order reaction might be considered as terminated when its rate is within a certain small percent (five percent, say) of the constant-rate reaction rate. The third term characterizes the on-going constant-rate reaction, with two model parameters A_c and E_{ac}. Although the first-order and constant-rate reactions are not tied to specific or identified reaction mechanisms, but rather are empirical descriptors of the overall reaction kinetics for which the many reactants participating in these reactions are unknown, the model fits the data quite well, as shown later.

In this model, six model parameters were identified: CA_{tank}, M, A_f, E_{af}, A_c, and E_{ac}. While CA_{tank} can be measured directly on tank asphalt, the other five are to be determined from analysis of kinetics data.

Using linear regression on the constant-rate data, k_c values were obtained as the slope of the constant-rate line at each aging temperature. The temperature dependency of k_c is shown in Figures 2.2, indicating a strong Arrhenius correlation. The activation energy of ALON PG64-22 is 83.2 KJ/mol, and the frequency factor is 3.68×10^{10} CA/day.

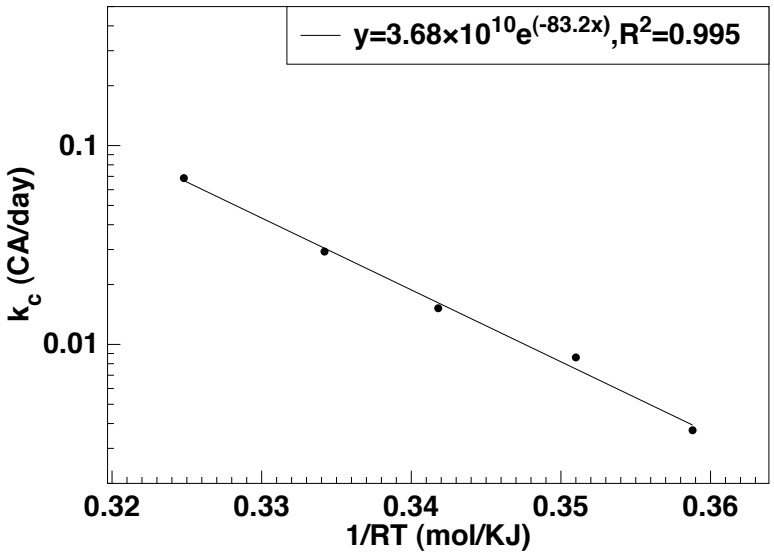

Figure 2.2. Temperature dependency of k_c values for Alon PG64-22.

Next, the constant-rate reaction kinetics parameters (activation energy and frequency factor) obtained from constant-rate data, and the average value of M ($CA_0 - CA_{tank}$, where CA_0 is the intercept of each constant-rate line) at five temperatures were used as initial values for optimization of all five model parameters. The objective of the optimization was to minimize the mean square error of model estimates of CA at all aging temperatures and times. The optimization is done using the *optim* function implemented in statistical software R (R Development Core Team, 2011).

This global optimization approach of the five model parameters worked well for all 15 binders. For each binder, this globally-optimal E_{ac} is within 0.12 KJ/mol of the

locally-optimal E_{ac}, determined from the constant-rate data only. These globally optimized parameters are listed in Table 2.3.

Table 2.3

Optimized Model Parameters for 20 Asphalts

Binder	CA_0	A_f (1/Day)	E_{af} (KJ/mol)	A_c (CA/Day)	E_{ac} (KJ/mol)
Alon PG 64-22	0.761	9.13×10^{7}	58.4	4.12×10^{10}	83.4
Alon PG 70-22	0.690	3.50×10^{8}	60.8	6.46×10^{9}	78.3
Alon PG 76-22	0.750	2.21×10^{7}	52.6	4.71×10^{9}	77.0
Lion PG 64-22	0.874	2.71×10^{9}	68.5	4.05×10^{11}	90.6
Martin PG 64-22	0.723	7.37×10^{6}	51.9	8.81×10^{8}	72.5
Martin PG 70-22	0.690	2.64×10^{8}	60.9	1.98×10^{11}	88.0
SEM PG 64-22	0.768	3.09×10^{6}	47.6	2.33×10^{8}	68.8
SEM PG 70-22	0.700	3.83×10^{7}	54.4	1.09×10^{10}	79.9
SEM PG 70-28	0.594	3.34×10^{7}	49.1	1.03×10^{9}	72.5
SEM PG 76-22	0.671	1.80×10^{6}	45.2	8.07×10^{7}	64.9
Valero-C PG 64-22	0.548	8.04×10^{9}	67.2	1.56×10^{11}	87.4
Valero-C PG 70-22	0.826	3.27×10^{10}	75.4	3.26×10^{13}	103.8
Valero-C PG 76-22	0.889	2.57×10^{6}	47.2	1.65×10^{8}	68.1
Valero-H PG 76-22	0.711	5.65×10^{9}	68.6	1.10×10^{11}	86.9
Valero-O PG 64-22	0.727	5.78×10^{7}	57.3	2.20×10^{10}	81.3
NuStar PG 67-22	0.752	1.04×10^{8}	55.8	3.70×10^{9}	76.1
NuStar PG 76-22	0.762	4.51×10^{6}	44.9	1.79×10^{8}	67.1
Valero-B PG 64-16	1.071	2.26×10^{8}	60.2	1.10×10^{11}	86.9
AAD-1	1.090	4.32×10^{8}	65.2	4.43×10^{11}	92.7
AAM-1	0.821	1.38×10^{8}	60.3	7.72×10^{10}	86.6

Using these five optimal model parameters for each asphalt, the proposed model provides calculations of carbonyl formation over time at each temperature that agree well with experimental measurements. This agreement validates the applicability of the empirical model for use in sophisticated pavement oxidation models to predict binder

oxidation in pavements. The comparison for Alon PG 64-22 (dashed lines) is shown in Figure 2.1. For the other binders, these comparisons are shown in Appendix A.

Analysis of Rheological Data

Low shear rate limiting viscosity for Alon PG 64-22 versus CA is shown in Figure 2.3 on a semi-log scale. For the other binders, the figures are presented in Appendix B. The same hardening susceptibility (HS, the slope of log complex viscosity versus CA) was observed for both fast-rate and constant-rate periods. These data also confirmed the observation made by Martin et al. (1990) that the HS was independent of aging temperature below 373 K. Based on these two important observations, changes in rheological properties (complex viscosity) are related to changes in chemical properties (CA), and therefore can be calculated using the proposed oxidation kinetics model for both fast-rate and constant-rate periods.

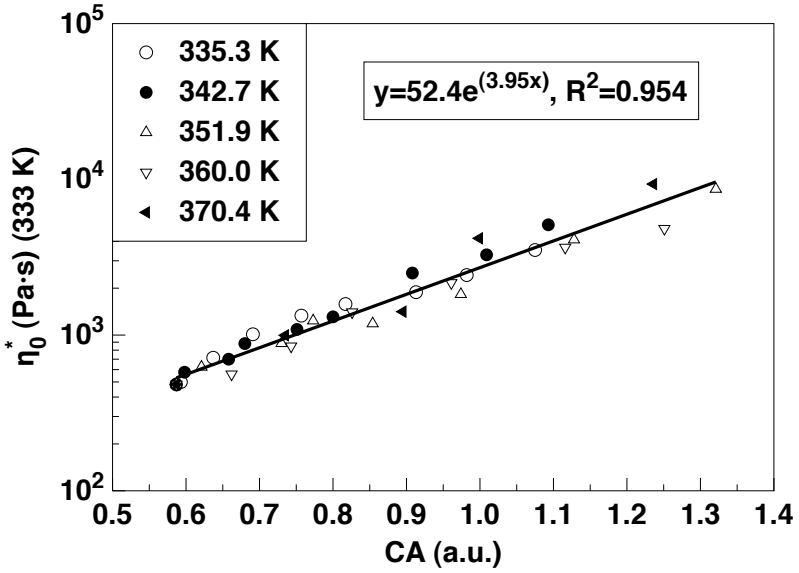

Figure 2.3. Limiting viscosity HS of Alon PG 64-22 for both fast-rate and constant-rate reactions.

Viscosity HS data for 15 binders were obtained and shown in Table 2.4. HS is dependent on asphalt composition, therefore each asphalt has a unique HS. Alon PG 64-22 and Alon PG 76-22, SEM PG 64-22 and SEM PG 76-22 shared the same base binders, respectively, but the others did not. The effect of SBS-polymer on HS is not clear because SBS-polymer modification increases the HS of the Alon base binder (from 3.95 to 5.03) but decreases the HS of the SEM base binder (from 4.86 to 3.73).

Table 2.4

Limiting Viscosity HS for 15 Asphalts

Binder	Viscosity HS (ln(Pa•s)/CA)
Alon PG 64-22	3.95
Alon PG 70-22 (SBS)	3.04
Alon PG 76-22 (SBS)	5.03
Lion PG 64-22	2.33
Martin PG 64-22	5.12
Martin PG 70-22 (SBS)	5.02
SEM PG 64-22	4.86
SEM PG 70-22 (SBS)	4.51
SEM PG 70-28 (SBS)	4.53
SEM PG 76-22 (SBS)	3.73
Valero-C PG 64-22	3.34
Valero-C PG 70-22 (SBS)	3.97
Valero-C PG 76-22 (SBS)	4.65
Valero-H PG 76-22 (SBS)	3.15
Valero-O PG 64-22	5.22

Sensitivity Analysis of Model Parameters

Comparing to the constant-rate kinetics model that considered only the third term in eq 2.2, three new parameters (M, A_f and E_{af}) were introduced into the kinetics model to characterize the fast-rate kinetics.

The M value represents the amount of aging due to the first-order reaction that terminates on the depletion of reactants. It significantly affects the accuracy of predicting the long-term constant-rate aging because it directly relates to the intercept of the constant-rate line, i.e. CA_0.

Given the M value and aging temperature, the rate constant for the fast-rate reaction determines how long the fast-rate period will last and affects the accuracy of predicting oxidation during this period. It was noted that the overall performance of model calculations at each aging temperature was not very sensitive to the fast-rate kinetics parameters. Figure 2.4 shows the sensitivity at one aging temperature to varying the M value and the fast-rate reaction constant k_f around their optimized values, for the Martin PG 64-22 binder. The M value was varied by ± 0.05, corresponding to the variation in the carbonyl area measurement. Reaction constant k_f was varied by ± 0.05 (1/day), corresponding to variation of the fast-rate activation energy by ± 10 (KJ/mol). Both M value and k_f were varied at a step size of 0.005. The root mean square errors (RMSE) of the model calculations were used to evaluate model performance. In Figure 2.4, at each fixed M value, the model performance (RMSE) changed slightly with k_f. However, M values showed a more significant impact. This analysis suggests that when the M value is accurately measured, the reaction constant k_f and equivalently the fast-rate activation energy E_{af}, as long as they are within an acceptable range, can be tolerated by the model without significantly affecting model performance. This argument provides support for a short-cut method of estimating fast-rate activation energies from constant-rate activation energies, discussed in the next section.

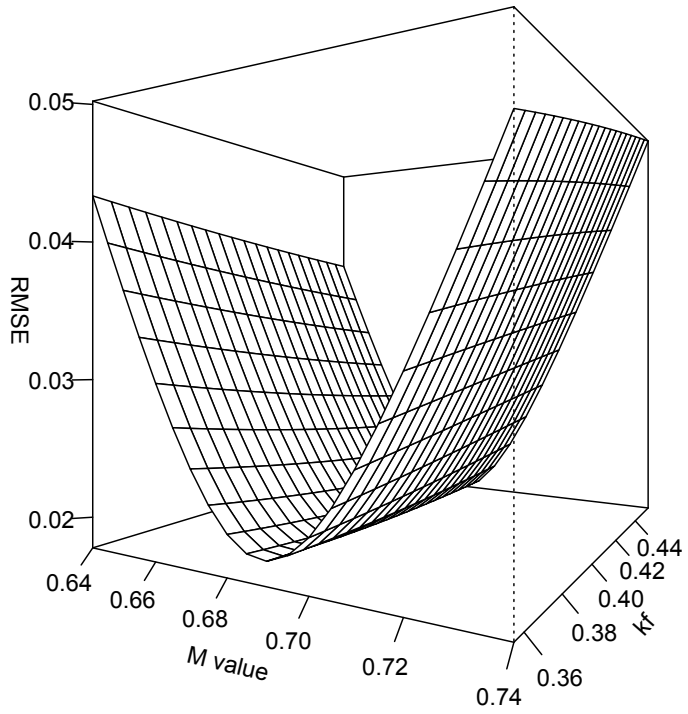

Figure 2.4. Sensitivity of model performance (expressed in terms of RMSE) to M and k_f.

Correlation between Fast-rate and Constant-rate Kinetics

Remarkably, the two activation energies, E_{af} and E_{ac} for all twenty asphalts plotted against each other in Figure 2.5, reveal a good linearity:

$$E_{af} = 0.82E_{ac} - 8.41 \quad (2.5)$$

The maximum error between E_{af} values calculated from E_{ac} values and the linear equation and E_{af} values obtained from optimization was 5.4 KJ/mol for the twenty binders, well within the ± 10 (KJ/mol) mentioned in the previous section. Therefore, it is suggested that this correlation can be used to estimate E_{af} from E_{ac}. Although it is an

empirical correlation with no apparent fundamental basis, it is of significant practical value, as explained in a later section.

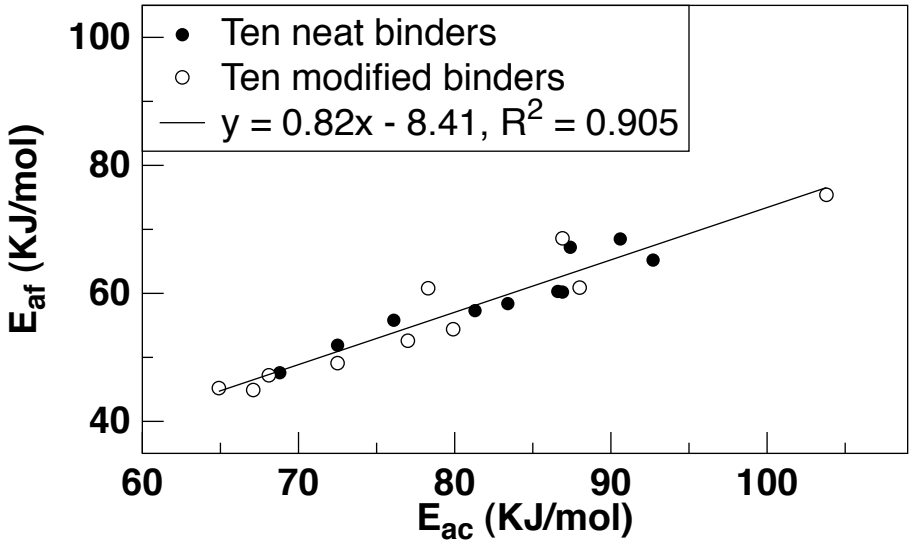

Figure 2.5. Empirical linear correlation between the fast-rate and constant-rate activation energies.

Correlation between Activation Energy and Frequency Factor

Domke et al. (2000) reported an isokinetic temperature of 378.2 K for constant-rate kinetics. At this temperature and 0.2 atmospheric oxygen partial pressure, all binders of different types showed the same aging rate during the constant-rate period. A similar temperature was obtained in this work. However, the activation energies in this work covered a broader range from 64.9 to 103.8 KJ/mol, while the range from Domke et al. (2000) was 82 to 90 KJ/mol. Furthermore, binders studied herein include SBS-modified

binders, and thus extends the concept of isokinetic temperature to polymer-modified binders.

Figure 2.6 shows the constant-rate activation energies and frequency factors on a semi-log scale for all twenty binders studied in this work, plus data of binders aged at 0.2 atmospheric oxygen partial pressure from Liu et al. (1996) and Domke et al. (2000). The correlation equation is:

$$A_c = 0.0428e^{0.3285E_{ac}} \quad (6)$$

The slope of the line is $1/RT_{iso}$ (mol/KJ) and the intercept (E_{ac} = 0) is the aging rate at T_{iso}. The isokinetic temperature T_{iso} is 366.1 K with an isokinetic aging rate of 0.0428 CA/day. This rate at the isokinetic temperature is useful in two aspects. First, it provides a universal aging rate for asphalts that is independent of its source and type, thus reducing the number of different temperatures by one at which experiments need to be conducted in order to make reasonable estimates of constant-rate kinetics parameters. Second, it provides the basis for ranking the pavement oxidation rates of asphalts by aging at only one elevated temperature, because the ranking at temperatures higher than T_{iso} will invert at temperatures lower than T_{iso}. However, it should be emphasized that oxidation rates alone cannot assess the superiority of binders, because different binders may show different hardening susceptibilities and thus different hardening rates.

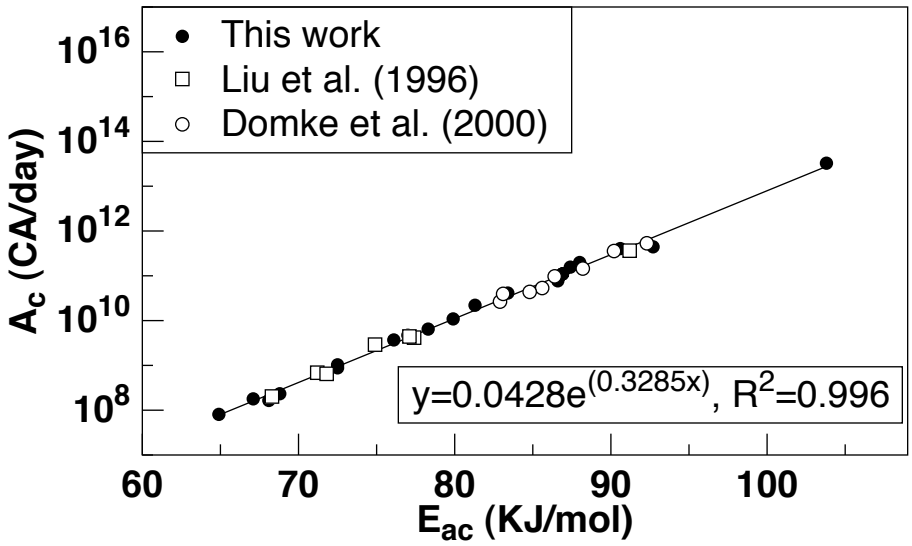

Figure 2.6. Isokinetic temperature 361.7 K of constant-rate reaction obtained from various data sources.

Interestingly, the fast-rate activation energies and logarithmic frequency factors for the 15 binders also show a linear correlation, Figure 2.7:

$$A_f = 2.031e^{0.3076E_{af}} \tag{7}$$

Note, however, that for a first order reaction the concept of an isokinetic temperature does not apply.

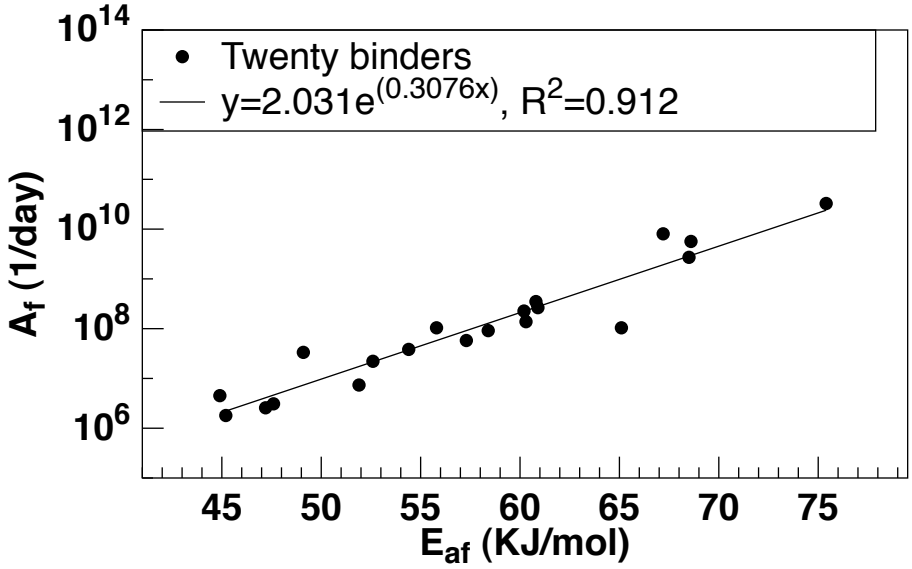

Figure 2.7. The correlation between fast-rate kinetics parameters.

A Simplified Asphalt Oxidation Kinetics Model

The asphalt oxidation kinetics model in eq 2.2 can be greatly simplified using the above three correlations of kinetics parameters. Given the constant-rate activation energy, the fast-rate activation energy can be calculated from eq 2.5, and the frequency factors A_f and A_c can be estimated from eqs 2.6 and 2.7. In this way, the total number of model parameters is reduced from six to three (CA_{tank}, M and E_{ac}).

Conclusions

The proposed "fast-rate, constant-rate" oxidation kinetics model described the experimental kinetics data quite well for all twenty asphalt binders, both neat and modified binders. Model parameters were obtained from global optimization. Sensitivity

analysis showed that the M value (the limiting about of oxidation product due to the fast-rate reaction) is a more sensitive parameter than the fast-rate rate constant.

Empirical correlations were found between model parameters. These correlations allow estimating fast-rate kinetics parameters from constant-rate kinetics parameters, reducing the number of model parameters from six to three: CA_{tank} (the carbonyl area of tank asphalt), M, and E_{ac} (the constant-rate activation energy). This reduction of parameters not only simplifies the kinetics model, but also saves the time and effort required to obtain the fast-rate oxidation kinetics data.

Rheological data confirmed previous reports that hardening susceptibilities of each binder were independent of aging temperature and aging period. With oxidative reaction kinetics parameters and hardening susceptibility, the proposed model was capable of predicting binder oxidation and hardening as a function of time and temperature. Such a capability is fundamentally important to pavement oxidation models, to improving pavement design, and to predicting pavement performance.

CHAPTER III

ASPHALT OXIDATION MECHANISM

Introduction

Several oxidation mechanisms of asphalt binder were reviewed in Chapter I. Specifically, they are Petersen's dual-reaction free radical chain reaction (FRCR) mechanism, King's oxycyclic electron transfer initiated oxidation (ETIO) mechanism, and Herrington's inhibited free radical autoxidation (IFRA) mechanism. All mechanisms have difficulty explaining the "fast-rate - constant-rate" scheme of binder oxidation. One possible reason is that reactions during the fast-rate period and the constant-rate period might go through different reaction pathways, therefore, no simple mechanism is able to explain the combined kinetics. One way to probe this possibility is by using antioxidants. By comparing the aging kinetics of antioxidant-treated binders with base (control) binders, the stage when the antioxidants take effect may be identified and the oxidation mechanism for the fast-rate period may be differentiated. For this purpose, a brief literature review of antioxidants was conducted.

In this chapter, one base binder and two antioxidants were selected for study. The base binder and the treated binders were aged at one temperature and air pressure. Then the effects of antioxidants on binder oxidation and on binder hardening were evaluated, respectively.

Antioxidants

The search of effective antioxidants to retard binder oxidation started as early as 1960. Through the years, many antioxidants were examined. Mainly, they were aromatic amines, metal (lead or zinc) compounds, phenolic antioxidants, carbon black, and hydrated lime (Apeagyei, 2006). The search and study of effective and economic antioxidants is still ongoing. For example, Willams et al. (2008) investigated lignin-containing ethanol co-products as an economic performance enhancer for asphalt. However, no universally effective antioxidant has been found to date.

During the evaluation of the effectiveness of antioxidants, very few people (Martin, 1968) studied the effect of antioxidants on binder oxidation chemistry. Most addressed the effectiveness of antioxidants based on comparison of rheological properties, typically viscosity. However, antioxidants might have changed the binder hardening in two aspects: 1) slowing down oxidation rates and 2) making the binder softer or harder by changing the binder composition and compatibility. Therefore, for the purpose of the mechanism study, these two aspects were studied separately.

Furthermore, while the oxidation of asphalt goes through an early fast-rate period then a later constant-rate period, most studies evaluated antioxidant-treated binders after RTFO (Rolling Thin Film Oven) aging and PAV (Pressure Aging Vessel) aging without considering these two different periods. It is possible that antioxidants only work during one of these two periods while the other is not affected. Therefore, binders were aged and sampled during both fast-rate and constant-rate period. This provided a chronological view of the function of antioxidants.

Materials

One binder (NuStar PG67-22) and two antioxidants were selected for this study. The two antioxidants were Irganox 1010 and Carbon Black. Irganox 1010 is a phenolic-type free radical scavenger, and carbon black is a multifunctional antioxidant that acts as both a free radical scavenger and peroxide decomposer. These two antioxidants were reportedly effective in hindering asphalt hardening (Apeagyei, 2010). Both antioxidants are non-toxic and thus are safer to handle than others such as lead and zinc compounds.

The base binder was treated with 0%, 1.5%, and 3.0% of antioxidants (by weight of binder). The treatment plan is shown in Table 3.1. "A" represents NuStar PG 67-22, "X" represents Irganox 1010, "C" represents Carbon Black, and "S" represents the mix of Irganox 1010 and Carbon Black (to see any possible effect of synergism).

Table 3.1
Treatment Plan of NuStar PG 67-22

Notation	Binder	Antioxidant (by Weight of Binder)
A	NuStar PG 67-22	-
AX1	NuStar PG 67-22	1.5% Irganox 1010
AX3	NuStar PG 67-22	3.0% Irganox 1010
AC1	NuStar PG 67-22	1.5% Carbon Black
AC3	NuStar PG 67-22	3.0% Carbon Black
AS	NuStar PG 67-22	1.5% Irganox 1010 and 1.5% Carbon Black

Experiment Methods

The base binder (control) and treated binders were aged in the pressure oxygen vessel (POV) at one elevated temperature (341K). Two replicate samples were collected at each sampling time (0, 3, 7, 10, 20 days). The sampling times were designed such that both fast-rate and constant-rate aging periods were observed.

Each sample was characterized using Fourier-Transform Infrared (FTIR) spectrometer and dynamic shear rheometer (DSR) for carbonyl area (CA) and low shear rate limiting viscosity, respectively. Details of these two methods were presented in Chapter II.

Results and Discussion

Effect of Antioxidants on Unaged Binders

The effects of antioxidants on unaged binders (both base binder and treated binders) were evaluated in terms of CA and viscosity, as shown in Table 3.2. AX1, AS, and AX3 showed higher CA than the base binder (A) did due to the four C=O in each Irganox 1010 molecule, while CAs of AC1 and AC3 were barely affected by the addition of Carbon Black. The low shear rate limiting viscosity was decreased by adding Irganox 1010, but increased by adding 3% carbon black. The effect of adding 1.5% carbon black on viscosity seemed to be small. The effect of additives on both chemical and viscous properties is interesting and relevant to the evaluation of antioxidant effectiveness.

Table 3.2
Properties of Neat and Treated Unaged Asphalts

Notation	CA	Limiting viscosity (@333K)
A	0.604	4514
AX1	0.739	4158
AX3	1.046	3582
AC1	0.658	4498
AC3	0.610	5971
AS	0.770	4798

Effect of Antioxidants on Oxidation Kinetics

Irganox 1010 is a phenolic-type free radical scavenger, and carbon black (Raven 790 from Columbia Chemical Company) is a multifunctional antioxidant that acts as both a free radical scavenger and peroxide decomposer. Both antioxidants were expected to be effective on binder hardening according to recent literature (Apeagyei, 2010). However, based on FTIR measurement of CA, both antioxidants, applied at different percentages and combined, had little effect of inhibiting or retarding binder oxidation. The kinetics of binder oxidation is the same with or without antioxidant treatment.

Figure 3.1 shows the trends of CA growth were the same for the base binder and the treated binders. The binders treated with Irganox 1010 (AX3, AX1, and AS) had

greater CA because of the ester group in the chemical structure of Irganox 1010. All treated binders followed the same fast-rate - constant-rate oxidation pattern as the base binder. This indicated two possibilities: 1) both fast-rate and constant-rate reactions did not follow the free radical chain reaction pathway, because free radical scavengers did not work for both fast-rate and constant-rate periods or 2) this reaction pattern was due to inhibited free radical reaction in which the pre-existed antioxidants in the base binder obscured the effect of added antioxidants. However, no future experiment was conducted to confirm any of these possibilities.

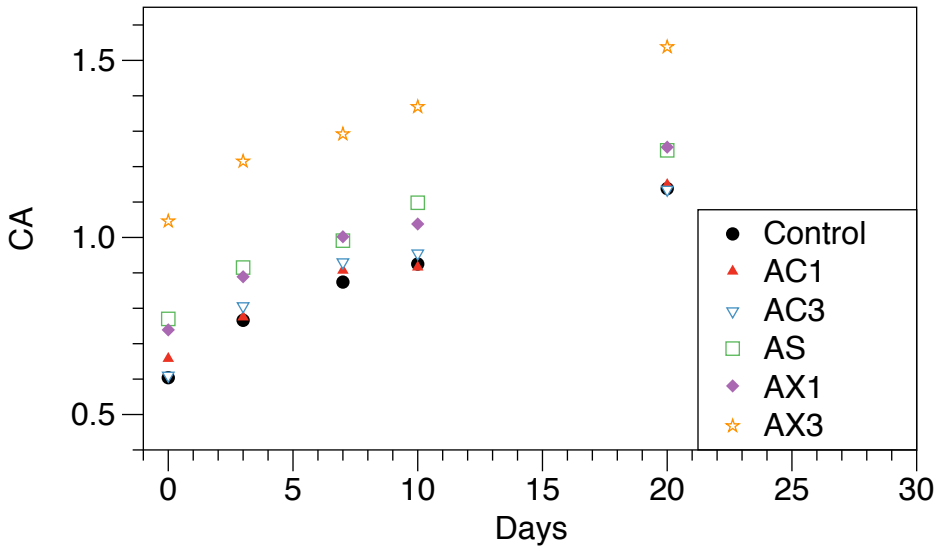

Figure 3.1. The trend of carbonyl area growth is the same for base binder and treated binders (aged at 341K).

Effect of Antioxidants on Binder Hardening and Hardening Susceptibility

Although the Irganox 1010 and carbon black were not effective in terms of carbonyl area, it was expected to have some effect on binder hardening based on aging index (Apeagyei, 2010). Therefore, the 60 °C low shear rate limiting viscosity was measured to investigate the effect of antioxidants on binder hardening and hardening susceptibility.

Figure 3.2 shows the viscosity with aging time for all binders. The treatment of 3% Irganox 1010 made the binder softer, while all other treatments showed little effect on viscosity. In terms of hardening rate, all antioxidant treatments are not effective. However, based on the aging index of viscosity, i.e. the ratio of viscosity of aged binder to viscosity of unaged binder, AC3 and AX1 were effective with aging indices of 1.29, smaller than that of the base binder (1.33). Therefore, the evaluation of antioxidant effective based on viscosity only could be misleading.

Figure 3.3 of viscosity versus CA showed the effect of antioxidants on of the hardening susceptibility. No significant difference in hardening susceptibility was observed, indicating that the binder's hardening response to oxidative aging was not significantly affected by antioxidants.

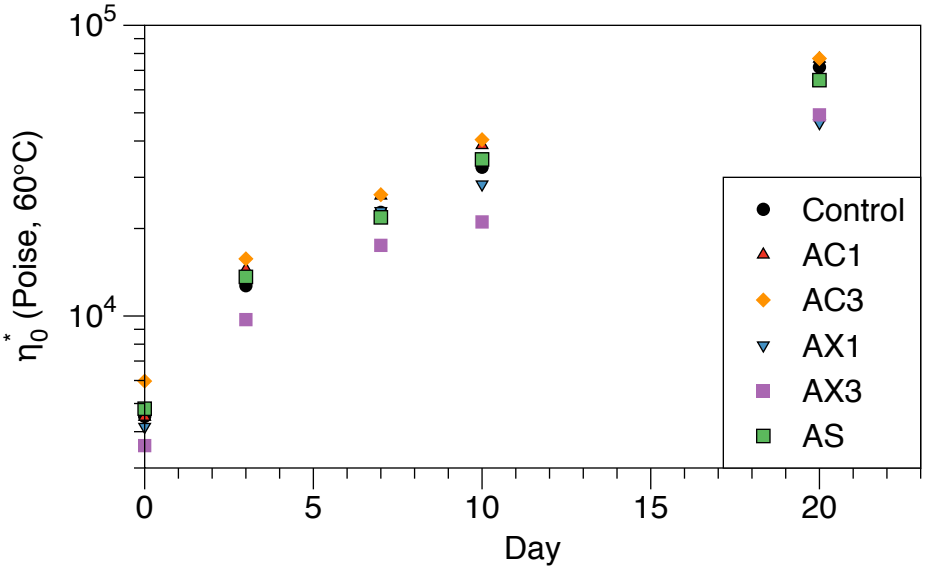

Figure 3.2. Viscosities of base and treated binders showed the same trend with aging (aged at 341K).

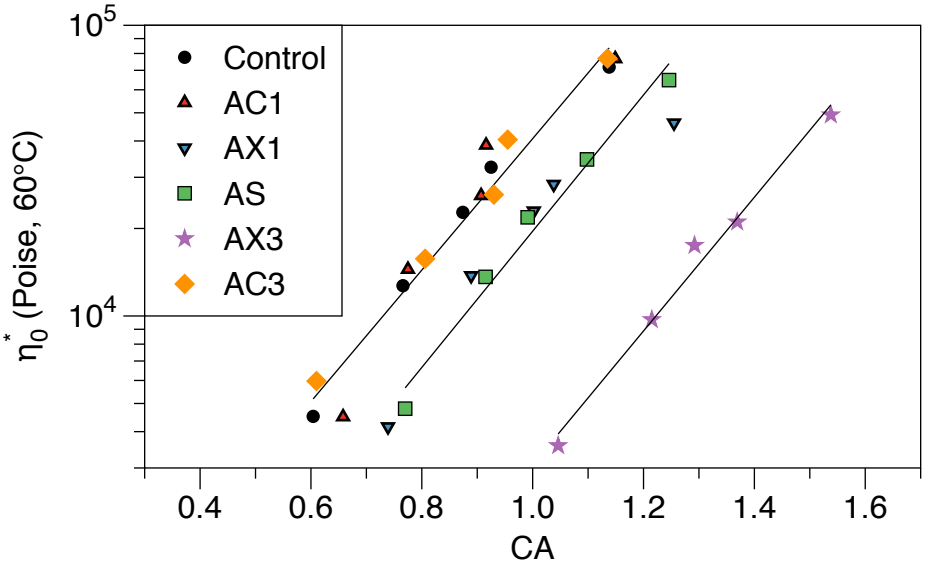

Figure 3.3. The hardening susceptibilities of base and treated binders are the same.

Summary

Two antioxidants (Irganox 1010 and Carbon Black) were investigated for the purpose of understanding asphalt oxidation mechanisms, especially for the early fast-rate reaction. Although these two antioxidants were reported to be effective through inhibiting free radical chain reactions, the results showed that they were not effective for the binder studied in this work. Therefore, no additional evidence was found to validate any of the proposed oxidation mechanisms in literature.

Results also suggested that evaluating antioxidant effectiveness based only on viscosity hardening could be misleading. A reliable evaluation should be based on the separate study of the antioxidant effectiveness on the oxidative reactions and on the hardening susceptibility of the treated binders.

CHAPTER IV

MODELING ASPHALT OXIDATION IN PAVEMENT WITH FIELD VALIDATION*

Introduction

The mechanistic-empirical pavement design guide (MEPDG) is being implemented by many state highway agencies (McCarthy et al., 2011). However, the global aging model (Mirza et al., 1995) used in MEPDG is problematic for predicting asphalt hardening in pavements. It fails to recognize that each binder has unique aging and hardening rates (Liu et al., 1996) and that asphalt oxidizes well below the top 25-mm of pavement (Al-Azri et al., 2006). Furthermore, it assumes that the level of oxidation in pavements has a practical limit, an assumption not supported by both laboratory and field data. In summary, a better model for asphalt oxidation in pavements is needed for both design and maintenance purposes.

Lunsford (1994) proposed a highway-pavement aging model, including important concepts such as oxygen diffusion limit, air voids, and binder content. Prapaitrakul et al. (2009) improved this model by using average pore radius,

---

*Parts of this chapter are reprinted with permission from "Modeling Asphalt Oxidation in Pavement with Field Validation" (manuscript ID: LPET-2012-0035.R1) by Xin Jin, Yuanchen Cui, Charles J. Glover. *Pet. Sci. Technol.* In press. Copyright by Taylor & Francis.

half-distance between two adjacent pores, and hourly pavement temperature input. Han (2011a) used five pore radii from X-ray CT measurements of pore size distribution instead of one average value, thus further refining the model.

In this chapter, the asphalt oxidation model was significantly improved by: 1) adding the concept of diffusion depth to better define the oxygen diffusion region in the mastic (a mixture of asphalt and fines); 2) incorporating both fast-rate and constant-rate asphalt oxidation kinetics; 3) introducing a field calibration factor to account for the factors not considered in the earlier models, for example, the tortuosity of oxygen path around aggregates, oxygen transport enhancement by micro cracks, and binder absorption by aggregates. Furthermore, the improved model was validated using field data and compared with the earlier models.

Model Development

Asphalt oxidation in pavements is a complex process of both oxygen and thermal transport. The pavement is produced by mixing aggregates and asphalts and then compacting the mixture to meet design requirements of air void content. Some of these air voids are trapped air voids while others are accessible air voids. Oxygen in accessible air void channels diffuses from these channels into asphalt films coating aggregate particles; meanwhile, oxygen reacts with asphalt, making the material stiffer and less permeable to oxygen. Both reaction and diffusion processes are affected by pavement temperature which is a function of time and depth.

These complex and interrelated processes were simplified for modeling purposes by making the following assumptions: 1) pavement temperature changes only in the

vertical direction, i.e. horizontal variation at the same pavement depth is negligible; 2) oxygen transports horizontally from pore wall into the mastic, i.e. no vertical diffusion; 3) at the pore wall, oxygen is at 0.2 atmospheric pressure, i.e. there is negligible oxygen transport resistance within the accessible air void channels from the pavement surface to lower pavement layers as supported by Han (2011a).

Model Components

Six components were included in the pavement oxidation model: 1) the oxygen transport-reaction model, representing how oxygen partial pressure (equivalent to concentration) changes as a function of position and time in the mastic, influenced by both oxygen diffusion and reaction; 2) the binder oxidation kinetics, describing the formation rate of carbonyl (the main oxidation product that contributes to asphalt hardening) as a function of temperature and oxygen partial pressure; 3) the oxygen diffusivity in the mastic, as a function of both temperature and binder viscosity (in turn influenced by asphalt composition, level of oxidation, and temperature); 4) the accessible air voids, providing the exposed surface area of asphalt to air; 5) mixture information, providing the volume of binder; 6) depth-dependent hourly pavement temperatures, as a driving force of pavement oxidation.

The first five components are discussed in more detail subsequently, whereas the pavement temperature model is detailed in the literature (Han et al., 2011b).

Accessible Air Void and Mixture Information

The accessible air void and mixture information are further discussed because they determine an average diffusion depth for oxygen into the mastic, important to the boundary condition for the oxygen transport-reaction model.

The diffusion depth is calculated from the exposed surface area of asphalt to accessible air voids (S_{ea}) and the volume of effective binder (V_{be}):

$$d_D = \frac{V_{be}}{S_{ea}} \tag{4.1}$$

where V_{be} is the total binder volume in the mix less the absorbed volume. This is similar to assuming that all binder surrounds accessible air voids at a uniform thickness, a reasonable first-order assumption for the purpose of asphalt oxidation. This assumption leads to a Cartesian system oxygen transport-reaction model. The concept of diffusion depth is different from the conventional asphalt film thickness, which is pictured as asphalt uniformly coating the aggregate surfaces. Because the exposed surface area of asphalt is much less than aggregate surface area, the magnitude of average diffusion depth will be greater than the film thickness.

The exposed surface area (S_{ea}) is estimated from the analysis of X-ray CT images of total air voids in the mixture. First, a series of grey-scale images of total air voids were obtained by scanning the field core from top to bottom at 1-mm intervals (Prapaitrakul et al., 2009). A threshold value, determined by matching the total air void content from the grey-scale images with that from measurement, converts the grey-scale images into binary images (Figure 4.1). Then the image processing toolbox in MATLAB was used to identify objects of connected air voids (Figure 4.2). Parts of these objects are

accessible air voids, depending on the pavement design. For example, if below the asphalt surface course is asphalt base, only objects connecting to the top image (i.e. pavement surface) are considered to be accessible air voids, while the other objects are consider to be trapped air voids with limited oxygen supply from the asphalt base. If below the asphalt surface course is unconsolidated base, objects connecting to the bottom image are also considered to be accessible air voids, the assumption being that atmospheric air is freely accessible through the unconsolidated base. After accessible air voids in each image are identified, the total perimeter of accessible air voids for each image (Figure 4.3) is obtained using MATLAB. If the same total perimeter for the 1-mm interval is assumed, the exposed surface area in that 1-mm interval is this perimeter times 1 mm. By applying this procedure to all images, the exposed surface area can be obtained for every image.

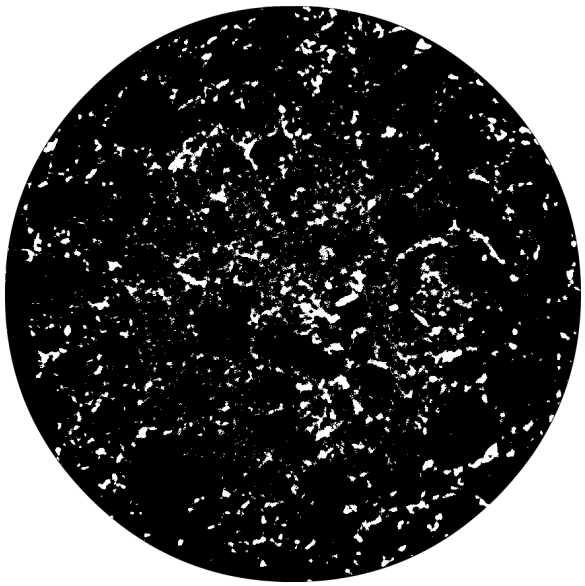

Figure 4.1. Binary image of total air voids in a field core (Black: Solid; White: Air Voids).

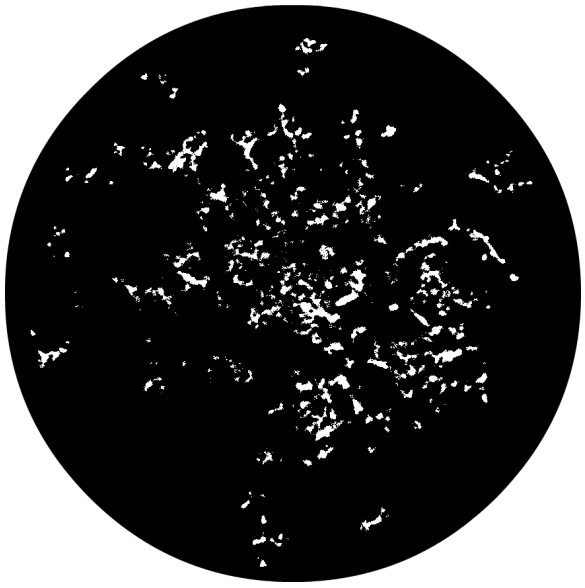

Figure 4.2. Binary image of accessible air voids in a field core (Black: Solid; White: Air Voids).

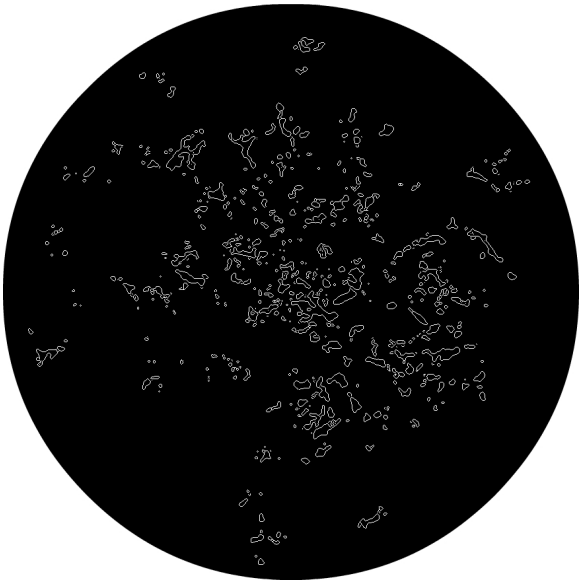

Figure 4.3. Highlighted perimeters of accessible air voids in a field core.

Furthermore, by summing the exposed surface areas of images belonging to a certain layer, the exposed surface area for that layer is obtained. Typically, about 50 images are obtained from a field core. The core can be sliced into several (4 to 5) asphalt layers and be studied layer-by-layer to understand the differences of surface area at different layer. The exposed surface area for a specific asphalt layer is

$$S_{ea}^{I} = \sum_{i \in I} S_{ea,i} = \sum_{i \in I} P_i \times 1 \tag{4.2}$$

where the superscript *I* represents the I-th asphalt layer, the subscript *i* represents the image that belong to the I-th layer, and P_i is the total perimeter of accessible air voids of the i-th image (mm).

The volume of the effective binder (V_{be}) is calculated from mixture information using the established volumetric procedure (Asphalt Institute, 2001). The mixture data needed include binder content (P_b, by weight of mixture), binder specific gravity (G_b), maximum specific gravity of the mixture (G_{mm}), total air void content (AV), and binder absorption (P_{ba}, by weight of aggregate). The equation is:

$$V_{be} = \frac{P_{be}}{100}\frac{W_{mix}}{G_b\,\gamma_w} = \frac{P_{be}}{100}\frac{G_{mm}V_{mix}}{G_b\,\gamma_w}\frac{100-AV}{100} \tag{4.3}$$

where V_{mix} is the volume of the field core, γ_w is the density of water, and P_{be} is the effective binder content by weight of mixture:

$$P_{be} = P_b - \frac{(100-P_b)}{100}P_{ba} \tag{4.4}$$

By assuming that the mixture design does not change with depth, the diffusion depth of oxygen for the Ith asphalt layer is calculated from:

$$d_D^I = \frac{V_{be}^I}{S_{ea}^I} \tag{4.5}$$

where V_{be}^I is the effective binder volume of the Ith asphalt layer.

Asphalt Oxidation Kinetics

Asphalt oxidation is characterized by the formation of carbonyl area (Liu et al., 1996). At constant temperature and oxygen pressure, the carbonyl area (CA) of asphalt undergoes an early nonlinear fast-rate period followed by a later constant-rate period (Van Oort, 1956; Liu et al., 1996; Herrington, 1998; Petersen et al., 1998). Data for recovered binder from field cores showed that the early fast-rate period may extend beyond hot-mix production (Glover et al., 2005), and an oxidation kinetics model for tank asphalt was developed to simulate both fast-rate and constant-rate reaction periods

(Jin et al., 2011). Herein, a similar model was assumed for short-term aged asphalt. The model consists of two parallel reactions: a first order reaction that terminates when the limiting amount of reactants is depleted, and a zero order constant-rate reaction that lasts indefinitely throughout the pavement service life. The equations for the growth of CA are:

$$\frac{\partial CA(x,t)}{\partial t} = M_{RTFO} k_f e^{-k_f t} + k_c \tag{4.6}$$

$$k_f = A_f P^{\alpha} e^{-E_{af}/RT} \tag{4.7}$$

$$k_c = A_c P^{\alpha} e^{-E_{ac}/RT} \tag{4.8}$$

where x is distance from the pore wall into surrounding mastic (meter), t is time (hour), M_{RTFO} is the limiting amount of carbonyl formation due to the first-order reaction after hot mix production, k_f and k_c are two reaction constants that are temperature dependent according to the Arrhenius equations, P is oxygen partial pressure (atm), and α is reaction order with respect to P. In this work, an average value 0.27 for α was used (Liu et al., 1996; Han et al., 2011a).

The initial condition is $CA(x, 0) = CA_{RTFO}$, i.e. the CA of asphalt after hot mix production. It may be obtained by testing binder after the rolling thin film oven (RFTO) or by testing the recovered binder of the loose mix from field.

Oxygen Transport-Reaction Model and Oxygen Diffusivity

The governing equation for the oxygen transport-reaction model is:

$$\frac{\partial P(x,t)}{\partial t} = \frac{\partial}{\partial x}\left(fcf \cdot D_O \frac{\partial P}{\partial x}\right) - \frac{c}{h} \cdot \frac{\partial CA(x,t)}{\partial t} \tag{4.9}$$

where D_O is oxygen diffusivity in pure asphalt (m^2/hour); *c* is a factor that converts rate of carbonyl formation to rate of oxygen consumption (mol O_2/[mL asphalt]/CA), with an average value of 3.71×10^{-4} based on ten asphalts (Liu et al., 1998) used in this work; *h* is the solubility constant of oxygen in asphalt (mol O_2/[mL asphalt]/[atm oxygen pressure in gas phase]), which is a function of temperature (Dickinson, 1984); *fcf* is the field calibration factor adjusting D_O. While the hindering effect of aggregates on oxygen diffusivity makes *fcf* less than unity, the assumption of no binder absorption and the development of cracks make *fcf* greater than unity. Therefore, *fcf* may be greater or less than unity due to the combined effect.

The initial condition is $P(x,0)=0$. The boundary conditions are $P(0,t)=0.2$, and $\frac{\partial}{\partial x}P(d_D,t)=0$, where d_D is the diffusion depth (meter).

The oxygen diffusivity (m^2/s) is a function of temperature and asphalt viscosity (Han et al., 2011c):

$$\frac{D_O}{T}=5.21\times10^{-12}LSV^{-0.55} \tag{4.10}$$

where *T* is temperature (Kelvin), and *LSV* is low shear rate limiting viscosity (Pa.s), which is a function that relates asphalt oxidation to hardening (Martin et al., 1990):

$$LSV=e^{m+HS\times CA} \tag{4.11}$$

where *m* is the intercept of ln(*LSV*) versus *CA*, and *HS* is the hardening susceptibility (ln(Pa.s)/CA). Both *m* and *HS* may be functions of temperature (Lunsford, 1994):

$$HS(T)\ =\ HS(T_0)+\gamma(\tfrac{1}{T}-\tfrac{1}{T_0}) \tag{4.12}$$

$$m(T)\ =\ m(T_0)+\sigma(\tfrac{1}{T}-\tfrac{1}{T_0}) \tag{4.13}$$

where T_0 is the reference temperature at which viscosities are measured (333 K in this work). γ = 1656 K/CA and σ = 20360 K, as averages of measured values. In general, although experimentally, *HS* is a very weak function of temperature.

The solubility of oxygen in asphalt is also a function of temperature (Dickinson, 1984):

$$h = 3.125\times10^{-6}[1 + 0.0215(T - 303)] \quad (4.14)$$

where T is temperature (K).

In equation 4.9, and considering a point in the asphalt mastic, the first term on the right-hand side represents the net input rate of oxygen to that point by diffusion and the second term represents the consumption rate of oxygen due to reaction with asphalt. These terms together give the accumulation rate of oxygen in the asphalt (the left side term). This equation and equation 4.6 form the system of partial differential equations for the pavement oxidation model.

Sensitivity Analysis of Model Parameters

In the pavement oxidation model, four model parameters are likely important to the prediction of long-term pavement aging and hardening: diffusion depth (d_D), field calibration factor (*fcf*), asphalt constant-rate activation energy (E_{ac}), and viscosity hardening susceptibility (*HS*). The model parameter M_{RTFO}, which defines the limiting amount of oxidation product due to first-order reaction after RTFO (or after hot-mix plant) aging, has a finite and transient effect during early pavement aging and hardening. A univariate sensitivity analysis was conducted with only the constant-rate reaction (eq.

4.8) for the first four model parameters. And to investigate the possible interactions between diffusion depth and field calibration factor, a multivariate sensitivity analysis was also conducted, with and without the fast-rate reaction.

Univariate Sensitivity Analysis

Three model parameters (d_D, E_{ac}, and HS) were varied based on the typical ranges of their measured or calculated values shown in Table 4.1. The range of field calibration factor was selected based on results to reflect its sensitivity. The set of values highlighted in bold was used as reference. When conducting the sensitivity analysis, only one model parameter was varied from its reference value while keeping the other parameters at their reference values.

Table 4.1
Values of Model Parameters Used in Univariate Sensitivity Analysis

Parameter	**Value**						
d_D (micron)	-	100	**500**	1000	2000	3500	5000
fcf (unitless)	0.01	0.05	**0.1**	0.25	0.5	1.0	4.0
E_{ac} (KJ/mol)	60	70	**80**	90	100	-	-
HS (ln(Pa•s)/CA)	-	2	**4**	6	-	-	-

Figure 4.4 to 4.7 show the results of the sensitivity analysis in terms of change in carbonyl area after 5 years of field aging assuming only the constant-rate reaction. Figure 4.4 shows that with the increase of diffusion depth, the change of carbonyl area (ΔCA) decreased. Furthermore ΔCA became much less sensitive to diffusion depth of

greater than 3000 microns, because the greater the diffusion depth is, the slower and more difficult for asphalt far away from the exposed surface to oxidize and the less the bulk average CA is affected. Dickinson (1984) drew a similar conclusion in a model calculation of diffusion-controlled reaction of oxygen with asphalt film.

Figure 4.5 shows that ΔCA increased with greater field calibration factor, indicating less diffusion resistance to oxygen diffusion through the mastic. Also ΔCA became less sensitive to a field calibration factor of greater than 0.5 for this case, indicating the process became reaction-rate controlled.

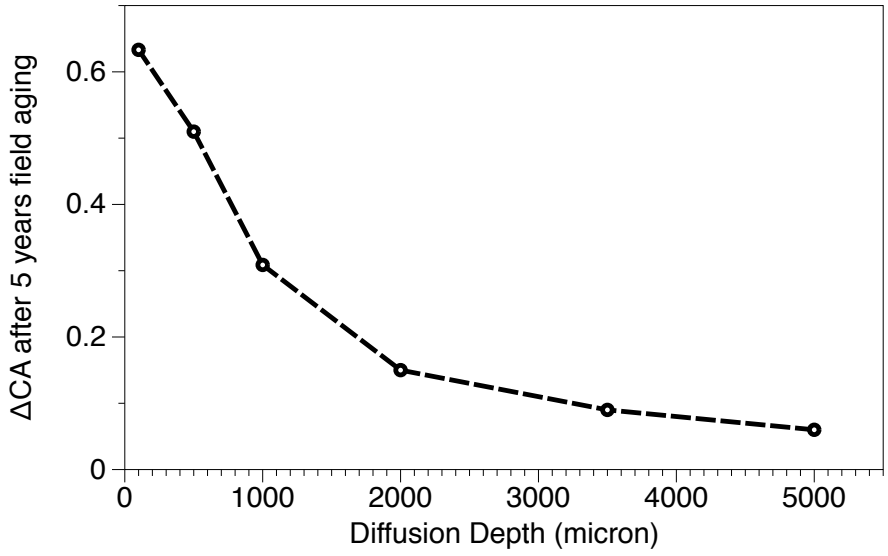

Figure 4.4. Sensitivity of carbonyl area increase to diffusion depth.

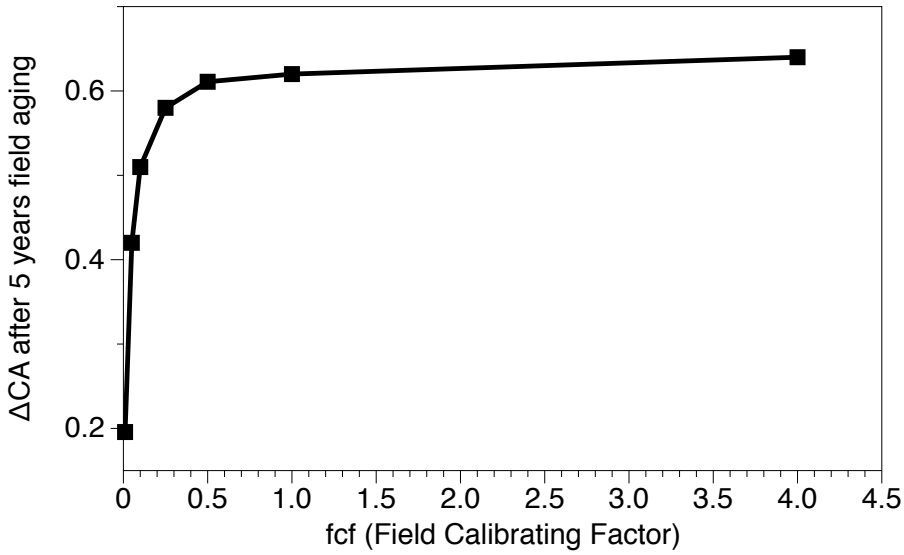

Figure 4.5. Sensitivity of carbonyl area increase to field calibration factor.

Figure 4.6 demonstrates the effect of asphalt constant-rate activation energy on oxidation. Lower activation energy represents higher oxidation rate, and ΔCA increased almost linearly with activation energy from 100 KJ/mol to 70 KJ/mol. For activation energies ranging from 60 to 70 KJ/mol, ΔCA showed less difference. This is probably due to the dominance of oxygen consumption by the oxidative reaction and that the formation of carbonyl area is mainly controlled by oxygen diffusion.

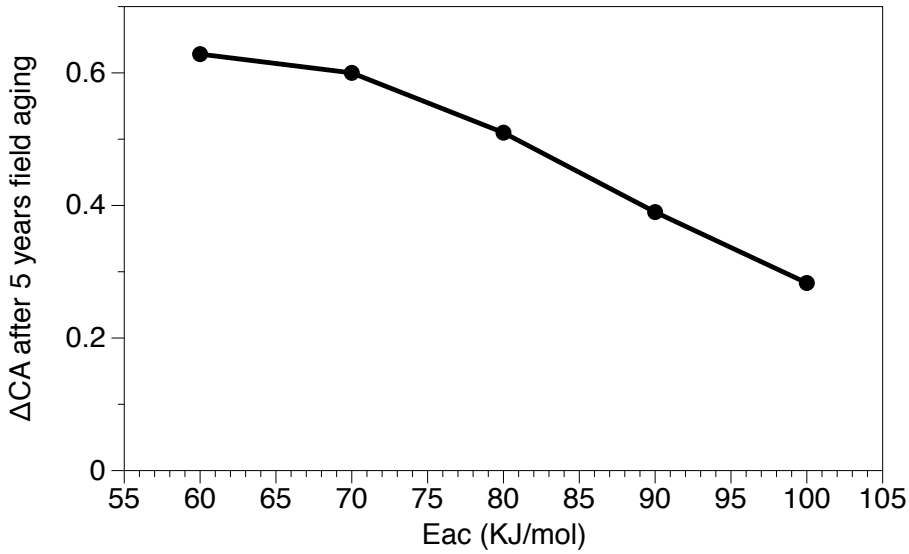

Figure 4.6. Sensitivity of carbonyl area increase to constant-rate activation energy.

Figure 4.7 shows the effect of viscosity hardening susceptibility on oxidation. The greater the HS is, the easier the asphalt hardens with oxidation, and the easier for asphalt at the exposed surface to form an asphalt skin that is less permeable to oxygen. As a result, oxidation is slowed down, suggesting that higher HS is preferred. However, greater HS means a greater tendency of asphalt hardening with respect to the same amount of carbonyl formation, making the asphalt more susceptible to cracking.

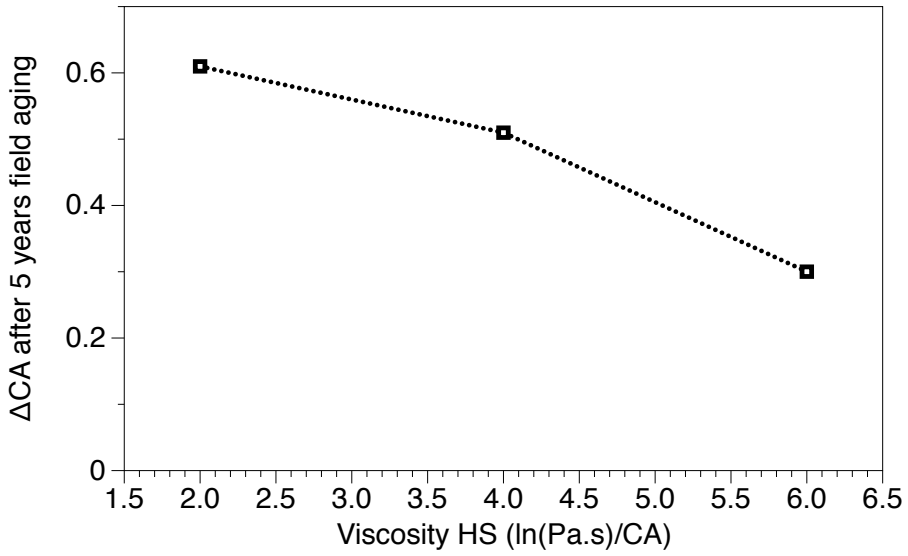

Figure 4.7. Sensitivity of carbonyl area increase to viscosity HS.

In short, all model parameters might be important depending on the reference state at which they are evaluated. And their effects on model output (i.e. the formation of carbonyl content) can be rationally explained.

Multivariate Sensitivity Analysis

The multivariate sensitivity analysis was conducted according to Table 4.2. The model parameters were varied at two to three levels for a total of 12 combinations. The other parameters (activation energy etc.) used the reference values shown in Table 4.1. The analysis was multivariate because the results were discussed for interaction between diffusion depth and field calibration factor, under two different conditions: one with no fast-rate reaction ($M_{RTFO} = 0$) and another with the fast-rate reaction ($M_{RTFO} = 0.2$).

Table 4.2
Values of Model Parameters Used in Multivariate Sensitivity Analysis

Parameter	Value		
d_D (micron)	500	2000	-
fcf (unitless)	4	10	20
M_{RTFO} (CA)	0	0.2	-

Figure 4.8 shows the sensitivity of carbonyl area increase (ΔCA) after five years of field aging to field calibration factor, at two levels of diffusion depth, with and without the fast-rate reaction. Clearly, ΔCA for M_{RTFO} = 0.2 (with the consideration of the fast-rate reaction) were higher than M_{RTFO} = 0. Note, according to the calculations for all 12 combinations, the ΔCA due to the fast-rate reaction reached M_{RTFO} before the end of five years. The difference in ΔCA, with and without the fast-rate reaction, was exactly 0.2 at the lower level of diffusion depth (500 micron) and high fcf values (10 and 20). However, for other cases, the differences were less than 0.2, indicating the ΔCA due to the constant-rate reaction were not the same. And the more diffusion resistance due to the combined effect of high diffusion depth and low fcf, the less ΔCA due to the constant-rate reaction.

Figure 4.8 shows the cases at the low level of diffusion depth (500 micron). The effect of field calibration factor was almost negligible, indicating the very low sensitivity of ΔCA to fcf. However, at the high level of diffusion depth (2000 micron), the ΔCA became more sensitive to field calibration factor at smaller fcf values.

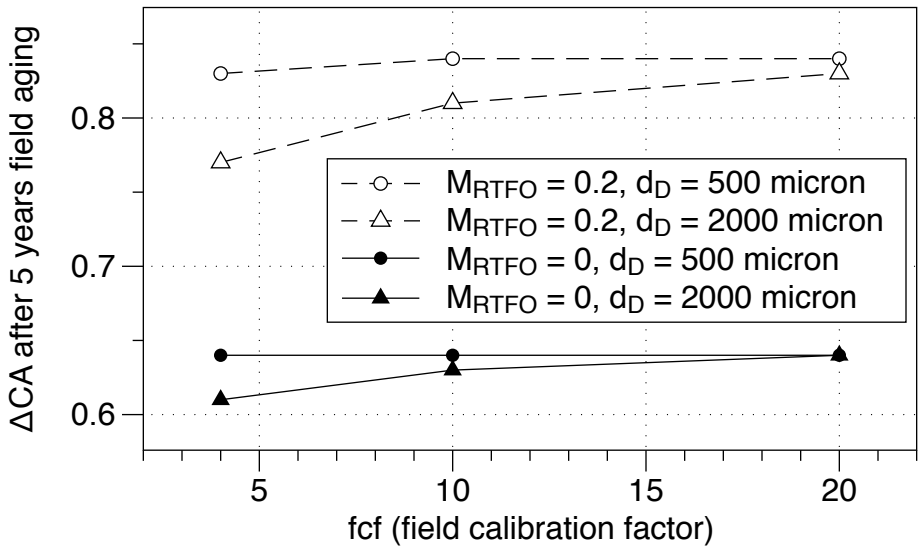

Figure 4.8. Sensitivity analysis of field calibration factor at different diffusion depth with and without fast-rate reaction.

Even more interesting is the convergence of the two sets of lines as the fcf increased. At higher fcf values, the ΔCA became less sensitive to diffusion depth.

In summary, both fcf and diffusion depth affects ΔCA by affecting oxygen diffusion resistance in the mastic. With the combination of high fcf value and low diffusion depth, the model behaves similarly to a thin film model, in which the effect of diffusion limitation is minimized.

Field Calibration and Validation of Pavement Oxidation Model

Materials

Field cores obtained from three field sites in Texas were used for model calibration and validation (Table 4.3). The three sites covered two different climate zones. Loose mixes were obtained during pavement construction. Two cores, one from a wheel path and another from the shoulder, were obtained from each site at each coring date, for a total of eleven cores.

Methodology

Oxidation kinetics parameters for the binders used in the field were obtained in the laboratory according to the method detailed by Jin et al. (2011). Binders in the loose mix were extracted and recovered, and values for CA_{RTFO} were measured. Next, total air void contents were measured for the field cores using the CoreLok method (Instrotek Inc., 2001). After that the field cores were scanned to obtain the grey-scale X-ray CT images, and then sliced into several (about 12mm thick) layers. The binders from each sliced layer were extracted and recovered for CA and viscosity measurements. The measured air void content, X-ray CT images, and mixture information were used to obtain the diffusion depth for each layer. These data (except X-ray CT images) are also shown in Table 4.3.

Table 4.3
Data of Field Cores, Binders, and Loose Mix

Route	**Location**	**Climate Zone**	**Constructed**	**Coring Dates**	**AV%**	**G_{mm}**
US 277	Del Rio, Texas	Dry-Warm	April 2008	1st: 7/28/2008 2nd: 12/14/2009	7.7	2.497
US 82	Lubbock, Texas	Dry-Cold	July 2008	1st: 8/25/2008 2nd: 12/9/2009	7.4	2.264
US 83	Childress, Texas	Dry-Cold	June 2008	1st: 8/15/2008 2nd: 10/22/2009	7.7	2.390
Route	**E_{ac} (KJ/mol)**	**HS (ln(Pa.s)/CA)**	**m (ln(Pa.s))**	**CA_{RTFO}**	**P_b**	**G_b**
US 277	75.2	3.97	5.84	0.740	4.2	1.041
US 82	69.6	3.33	6.04	0.814	6.2	1.021
US 83	72.5	4.53	7.89	0.526	5.3	1.020

* G_{mm}, P_b, and G_b are provided by mixture design.

Site-specific hourly pavement temperatures for an entire year were calculated using the pavement temperature model developed by Han et al. (2011b). These calculations were used repeatedly assuming they adequately represent pavement temperatures over the other years.

The CA data for the top two layers of the second shoulder cores were used for calibrating the two model parameters: *fcf* and M_{RTFO}. The other CA data for first and second cores (from both wheel path and shoulder) were used for model validation.

Results and Discussion

Table 4.4 presents the diffusion depths, measured CA data, and model calculations for the three pavement sites. The recovered binder CA data of the loose mix and the top two layers of shoulder second cores (bolded in Table 4.4) were used for parameter calibration of *fcf* and M_{RTFO}. For US 277, the optimal values for *fcf* and M_{RTFO} are 1.2 and 0.05, respectively. For US 82, the optimal values for *fcf* and M_{RTFO} are 10 and 0.18, respectively. For US 83, the optimal values for *fcf* and M_{RTFO} are 12 and 0.12, respectively. Because no binder absorption data were available for these two sites, zero binder absorption was assumed, making *fcf* greater than unity.

Table 4.4
Layer-by-layer Diffusion Depth (mm) and CA of US 277, US 82 and US 83 Field Cores

Layers of	Wheel Path 1st Core			Wheel Path 2nd Core		
US 277	**d_D (mm)**	**CA data**	**CA calc**	**d_D (mm)**	**CA data**	**CA calc**
1	0.386	0.936	0.961	1.167	1.206	1.110
2	0.615	0.937	0.934	3.072	1.004	0.906
3	0.748	0.971	0.911	0.575	0.970	1.131
4	0.706	0.955	0.901	0.510	0.886	1.106
5	0.462	0.930	0.907	-	-	-
US 82	**d_D (mm)**	**CA data**	**CA calc**	**d_D (mm)**	**CA data**	**CA calc**
1	0.974	0.879	0.972	1.293	1.201	1.193
2	2.948	0.83	0.868	2.037	1.122	1.063
3	4.360	0.823	0.843	1.846	1.193	1.032
4	3.292	0.831	0.845	-	-	-
US 83	**d_D (mm)**	**CA data**	**CA calc**	**d_D (mm)**	**CA data**	**CA calc**
1	0.847	0.898	0.968	1.297	1.094	1.128
2	4.405	0.791	0.867	2.346	0.994	1.011
3	3.146	0.798	0.871	1.802	0.981	1.028
Layers of	**Shoulder 1st Core**			**Shoulder 2nd Core**		
US 277	**d_D (mm)**	**CA data**	**CA calc**	**d_D (mm)**	**CA data**	**CA calc**
1	0.663	1.019	0.950	**0.592**	**1.218**	1.240
2	0.636	0.897	0.933	**2.710**	**0.959**	0.918
3	0.790	0.894	0.908	1.579	0.971	0.960
4	0.603	0.923	0.909	0.675	0.949	1.074
5	0.344	0.918	0.913	0.700	1.008	1.039
US 82	**d_D (mm)**	**CA data**	**CA calc**	**d_D (mm)**	**CA data**	**CA calc**
1	0.970	0.876	0.972	**0.883**	**1.218**	1.219
2	3.111	0.771	0.866	**2.550**	**1.015**	1.013
3	3.768	0.798	0.847	11.362	1.026	0.850
4	-	-	-	6.367	1.109	0.863
US 83	**d_D (mm)**	**CA data**	**CA calc**	**d_D (mm)**	**CA data**	**CA calc**
1	-	-	-	**0.966**	**1.102**	1.105
2	-	-	-	**3.032**	**0.949**	0.937
3	-	-	-	2.778	0.934	0.983
4	-	-	-	2.026	0.934	1.038
5	-	-	-	1.267	0.948	0.892

Using the calibrated model parameters, CA values of the other layers of both first and second cores were calculated using the pavement oxidation model. Figure 4. 9 compares the model calculations with data layer by layer for US 277 shoulder. The model calculations matches with data of all layers quite well. The top and bottom layers of second core oxidized significantly greater than the second and third layers, due to much smaller diffusion depths (0.592 and 0.700 mm) of the former layers versus 2.710 and 1.579 mm for in the latter layers. Furthermore, the top layer oxidized the most due to the highest temperature at the pavement surface. These data demonstrates the capability of the model to predict the oxidation of asphalt in pavement at different depths.

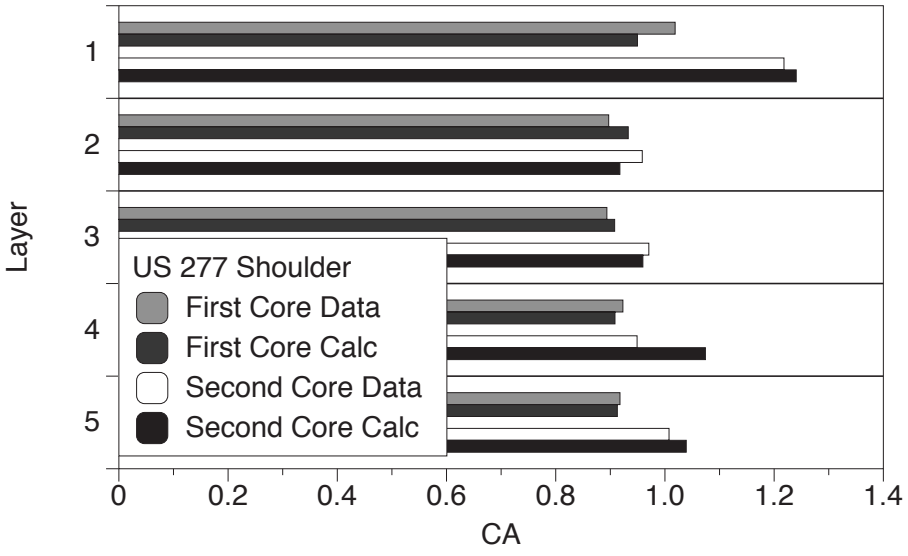

Figure 4.9. Comparison of field data and model estimates of CA for US 277 shoulder.

Figure 4.10 compares calculations of CA averaged over the whole core for US 277 shoulder. The models compared were 1) the model developed in this work; 2) the thin film model based on this model but assuming no oxygen diffusion resistance in the binder; 3) Han's model that did not include a fast-rate period. The stepwise increases reflect seasonal changes in pavement temperatures. The thin film model agreed with the first-core data point, however, it overestimated the oxidation at later times when diffusion resistance increases due to age hardening. The calculation of Han's model was based on his calculated average yearly oxidation rate for this pavement site (Han, 2011a). Clearly, it did not capture the fast oxidation during the early period. Calculations of the model developed in this work using diffusion depths of the second core showed that the oxidation rate declined over time due to increased diffusion resistance. And the discrepancy between the first-core data point and the model calculation was because the actual diffusion depth of the first core was less than that of the second core, which was used for the calculation.

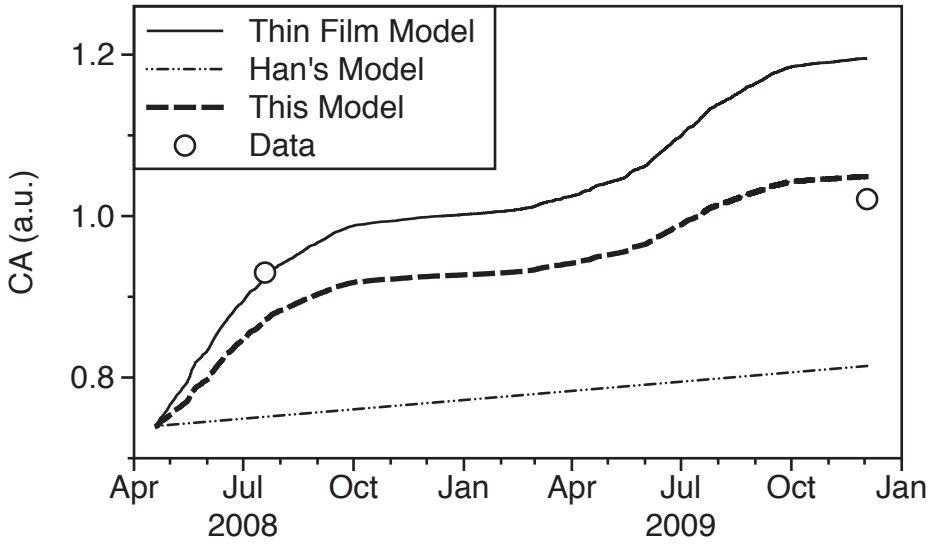

Figure 4.10. Comparison of CA calculations using different models for US 277 shoulder.

In summary, a total of 44 model predictions were made for the 44 layers of eleven cores. In general, the model predicts asphalt oxidation in pavement as a function of time and depth quite well. Figure 4.11 shows a box plot of percent error of the model predictions. 82% of the percent errors were within ±11% of CA data. Using a common value of hardening susceptibility (5 ln(Pa.s)/CA), 11% error in CA leads to about 5% error in ln(*LSV*). Part of the discrepancy between data and estimates was due to measurement error (about 5%). Other factors include the effect of asphalt absorption on diffusion depth and change of air voids content over time due to traffic compaction and crack development.

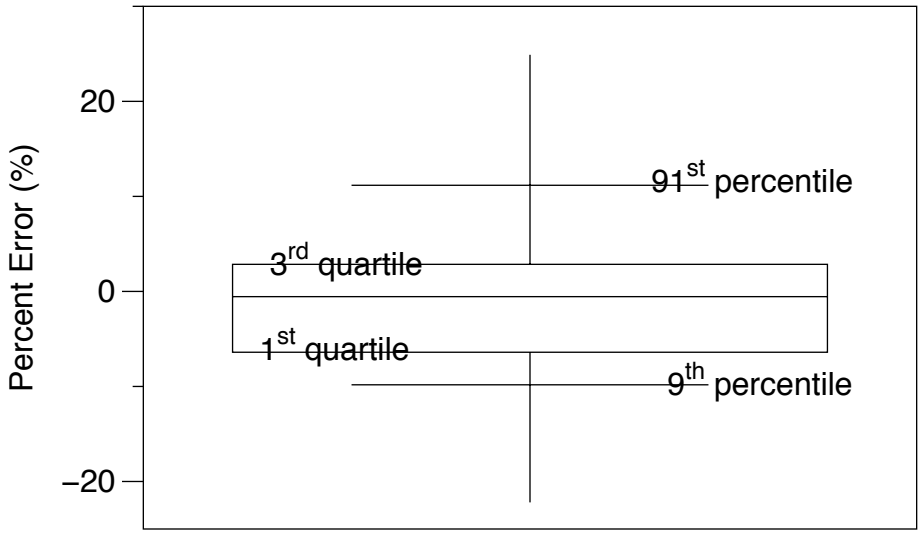

Figure 4.11. Box plot of percent errors of 44 CA estimates.

Conclusion

A pavement oxidation model was developed based on oxygen transport and reaction fundamentals. It requires binder oxidation kinetics and hardening parameters for both fast-rate and constant-rate reaction periods, calibrated oxygen diffusivity in the mastic, accessible air voids characterization of the mixture, and mixture information. The model also requires the input of hourly pavement temperatures. Two model parameters M_{RTFO} and *fcf* were calibrated using field data. And the model was capable of predicting asphalt oxidation in pavements after one year of field aging quite well.

CHAPTER V

CONCLUSIONS AND FUTURE RESEARCH

Asphalt oxidation kinetics and asphalt oxidation in pavements was extensively investigated in this dissertation. Understanding asphalt oxidation kinetics for both fast-rate and constant-rate periods is essential to the development of a pavement oxidation model. And modeling asphalt oxidation in pavements is important for predicting pavement oxidation and hardening under realistic environmental conditions, and is useful for pavement design and determining optimal maintenance timing. This chapter summarizes the important findings and suggested future research.

Asphalt Oxidation Kinetics Model

The asphalt oxidation in the laboratory at constant temperature and constant oxygen pressure showed a nonlinear early fast-rate period followed by a later constant-rate period. This behavior was modeled by two parallel reactions, a first-order fast-rate reaction and a zero-order constant-rate reaction. A fast-rate – constant-rate reaction kinetics model was developed and was able to fit experimental data quite well for both neat and modified binders. The model describes asphalt oxidation in terms of carbonyl formation, as a function of time, temperature, and oxygen partial pressure. With hardening susceptibility, the model also predicts asphalt oxidative hardening.

Further investigation of model parameters of the fast-rate reaction and the constant-rate reaction revealed interesting correlations between the kinetics parameters. And these correlations are valid for both neat and modified binders. Using these

correlations, the number of parameters to be measured is reduced from six to three, and the experimental efforts and time are significantly reduced.

Future work is suggested to further extend the application of the kinetics model. The pressure dependence of *M* suggests that the frequency factor of the fast-rate reaction probably is also a function of oxygen partial pressure. It will also be very interesting to develop an efficient method of estimating *M* from the analysis of asphalt composition rather than from experiments. Domke et al. (2000) suggested that *M* value might be related to asphalt composition (heptane asphaltenes and pentane ratio). If such a correlation was established, *M* value might be obtained through the relative short compositional analysis; on the contrary, measuring *M* value (as the intercept of constant-rate data) from oxidative reaction experiment is time-consuming.

In terms of field application, the *M* value should be measured after short-term aging such as RTFO that simulates hot-mix plant aging. The applicability of the kinetics model for binders after short-term aging should also be validated. Furthermore, it is interesting to compare the *M* value obtained for unaged binder and the *M* value obtained for the same binder after short-term aging.

Asphalt Oxidation Mechanism

The purpose of the study of the oxidation mechanism was to understand why the fast-rate and constant-rate reactions might be correlated. Two antioxidants, reported to be effective based on recent literature, were selected and studied. However, both fast-rate and constant-rate reactions were not significantly affected by the treatment of both antioxidants. Although the asphalt oxidation mechanism is still unclear, experimental

results showed that in order to draw reliable conclusions, it is essential to evaluate the effect of antioxidant on oxidation rate and on hardening susceptibility independently.

Pavement Oxidation Model

The pavement oxidation model incorporated the asphalt oxidation kinetics model and the oxygen transport model in the mastic, and considered the supply of oxygen from accessible air voids and the effect of changing pavement temperature. A critical model parameter is the diffusion depth, which characterizes the average diffusion depth of oxygen into the mastic and reflects the effect of air voids and binder content. Sensitivity analysis of model parameters indicated that at certain threshold values of field calibration factor and diffusion depth, the asphalt oxidation process becomes reaction controlled, i.e. the model results approaches that of a thin-film model calculation with no oxygen diffusion limitation. Two parameters in the model M_{RTFO} and field calibration factor were estimated using field data. And the model was validated using data of field cores aged in pavement up to one year. Ultimately, this model can be used with pavement response models in a pavement design guide for evaluating long-term pavement performance.

The following future work is suggested:

1. Extended validation of the model with data from field cores that are aged in the field for two and three years.
2. Investigation of field data variability. Each field measurement at each point in time was obtained from a single core with no replicate. Duplicate field core, if

available, should be studied to investigate the statistical variability of field data, to better quantify the model accuracy.

3. A simplified method for air void characterization and diffusion depth analysis. In this work, air void information was obtained from X-ray CT images. A simpler and more economic approach would be to correlate diffusion depth to certain bulk properties of the mixture, such as compaction level or total air voids.
4. Measurement of M_{RTFO} using POV aging of RTFO aged binder or recovered binder from loose mix. In this work, this parameter was estimated from field data.
5. A better characterization of the factors accounted by the single field calibration factor. The field calibration factor accounts for several aspects, including the hindering effect of small aggregate particles on oxygen diffusion, the absorption of binder by aggregates leading to less diffusion depth than actually used in calculation, the change of accessible air voids due to traffic compaction and crack development which leads to change in diffusion depth.

REFERENCES

Al-Azri, N. A., Jung, S. H., Lunsford, K. M., Ferry A., Bullin, J. A., Davison, R. R., and Glover, C. J. (2006). Binder Oxidative Aging in Texas Pavements: Hardening Rates, Hardening Susceptibilities, and Impact of Pavement Depth. *Transp. Res. Rec.* 1962:12–20.

Anderson, D. A., Christensen, D. W., Bahia, H. U., Dongre, R., Sharma, M. G., Antle, C. E., and Button, J. (1994). *Binder Characterization and Evaluation, Volume 3: Physical Characterization*. SHRP Report A-369. Washington, D.C.: Strategic Highway Research Program/National Research Council.

Apeagyei, A. K. (2006). *Laboratory Evaluation of Antioxidants for Asphalt Binders.* Ph.D. dissertation. Champaign, Illinois: University of Illinois at Urbana-Champaign.

Apeagyei, A. K. (2010). Laboratory Evaluation of Antioxidants for Asphalt Binders. *Constr. Build. Mater.* 25:47-53.

Asphalt Institute. (1994). *Performance Graded Asphalt Binder Specification and Testing.* SuperPave series No. 1 (SP-1). Lexington, Kentucky: Asphalt Institute.

Asphalt Institute. (2001). *Superpave Mix Design.* Superpave Series No. 2 (SP-2). Lexington, Kentucky: Asphalt Institute.

Beaver, B. D., and Gilmore C. (1991). Oxidative Degradation of Petroleum Products Via A Non-peroxyl Radical Chain Pathway: Electron Transfer Initiated Oxidation (ETIO) Revisited. *Pet. Sci. Technol*. 9:811-823.

Branthaver, J. F., Petersen, J. C., Robertson, R. E., Duvall, J. J., Kim, S. A.,

Harnsberger, P. M., Mill, T., Ensley, E. K., Barbour, F. A., and Schabron, J. F. (1993). *Binder Characterisation and Evaluation, Volume 2 Chemistry*. SHRP Report A-368. Washington, D.C.: Strategic Highway Research Program/National Research Council,.

Cortez, E. M. (2009). *Environmental Conditions and Binder Aging Characteristics in the Intermountain Region of the United States.* M.S. Thesis. Reno, Nevada: University of Nevada-Reno.

Dickinson, E. J. (1984). The diffusion controlled reaction of oxygen with films of bituminous binders. *Aust. Road Res.* 14:121-132.

Domke, C. H., Davison R. R., and Glover, C. J. (1999). Effect of Oxidation Pressure on Asphalt Hardening Susceptibility. *Transp. Res. Rec.* 1661:114-121.

Domke, C. H., Davison R. R., and Glover, C. J. (2000). Effect of Oxygen Pressure on Asphalt Oxidation Kinetics. *Ind. Eng. Chem. Res.* 39:592-598.

Glover, C. J., Davison, R. R., Domke C. H., Ruan Y., Juristyarini P., Knorr D. B., and Jung S. H. (2005). *Development of a New Method for Assessing Asphalt Binder Durability with Field Validation*. Publication FHWA/TX-05/1872-2. College Station, Texas: Texas Transportation Institute.

Glover, C. J., Epps Martin, A., Chowdhury, A., Han, R., Prapaitrakul, N., Jin, X., and Lawrence, J. (2009). *Evaluation of Binder Aging and Its Influence in Aging of Hot Mix Asphalt Concrete: Literature Review and Experimental Design*. Publication FHWA/TX-08/0-6009-1. College Station, Texas: Texas Transportation Institute.

Han, R. (2011a). *Improvement to A Transport Model of Asphalt Binder Oxidation in*

Pavements: Pavement Temperature Modeling, Oxygen Diffusivity in Asphalt Binders and Mastics, and Pavement Air Void Characterization. Ph.D. dissertation. College Station, Texas: Texas A&M University.

Han, R., Jin, X., and Glover, C. J. (2011b). Modeling of Pavement Temperature History for Use in Binder Oxidation Models and Pavement Performance Prediction. *J. Mater. Civ. Eng.* 23:351-359.

Han, R., Jin X., and Glover, C. J. (2011c). Oxygen Diffusivity in Asphalts and Mastic. *Pet. Sci. Technol.* In press.

Hajj, E. Y., Sebaaly, P. E., and Weitzel, D. (2005). Fatigue Characteristics of Superpave and Hveen Mixtures. *J. Transp. Eng*. 131:302-310.

Herrington, P. R. (1998). Oxidation of Bitumen in the Presence of a Constant Concentration of Oxygen. *Pet. Sci. Technol.* 16:1061-1084.

Herrington, P.R. (2004). Effect of Oxygen Concentration on the Rate of Reaction of Asphaltenes with Oxygen. *Energy Fuels*, 18:1573-1577.

InstroTek Incorporated. (2001). *Corelok® Operator's Guide*, *Version 10.* Raleigh, North Carolina: InstroTek Incorporated.

Jemison, H. B., Burr, B. L., Davison, R. R., Bullin, J. A., and Glover, C. J. (1992). Application and Use of the ATR, FT-IR Method to Asphalt Aging Studies. *Fuel Sci. and Technol.* 10:795-808.

Jin, X. (2009). *Contributions to an Improved Oxygen and Thermal Transport Model and Development of Fatigue Analysis Software for Asphalt Pavements.* M.S. thesis. College Station, Texas: Texas A&M University.

Jin, X., Han, R., Cui, Y., and Glover, C. J. (2011). Fast-Rate – Constant-Rate Oxidation Kinetics Model for Asphalt Binders. *Ind. Eng. Chem. Res.* 50:13373-13379.

King, G. N. (1993). Oxycyclics: understanding catalyzed oxidation mechanisms in bitumen and other petroleum products. *Pet. Sci. Technol.*, 11:201-238.

Knotnerus, J. (1972). Bitumen Durability – Measurement by Oxygen Absorption. *Ind. Eng. Chem. Prod. Res. Develop.* 11:411-422.

Lau, C. K., Lunsford, K. M., Glover, C. J., Davison, R. R., and Bullin, J. A. (1992). Reaction Rates and Hardening Susceptibilities as Determined from POV Aging of Asphalts. *Transp. Res. Rec.* 1342:50-57.

Liu, M., Lunsford, K. M., Davison, R. R., Glover, C. J., and Bullin, J. A. (1996). The Kinetics of Carbonyl Formation in Asphalt. *AIChE J*. 42:1069-1076.

Liu, M., Ferry, M. A., Davison, R. R., Glover, C. J., and Bullin, J. A. (1998). Oxygen uptake as correlated to carbonyl growth in aged asphalts and asphalt Corbett fractions. *Ind. Eng. Chem. Res.* 37:4669-4674.

Lunsford, K. M. (1994). *The Effect of Temperature and Pressure on Laboratory Oxidized Asphalt Films with Comparison to Field Aging*. Ph.D. dissertation. College Station, Texas: Texas A&M University.

Martin, K. G. (1966). Influence of Stabilizers on Bitumen Durability. *J. Appl. Chem.* 16:197–202.

Martin, K. L., Davison, R. R., Glover, C. J., and Bullin, J. A. (1990). Asphalt Aging in Texas Roads and Test Sections. *Transp. Res. Rec.*, 1269:9-19.

McCarthy, L. M. and Liang, J. (2011). *Sensitivity Analysis for Flexible Pavement Design*

Using the Mechanistic-Empirical Pavement Design Guide. Transportation Research Circular, E-C155. Washington D.C.: Transportation Research Board.

Mirza, M. W. and Witczak, M.W. (1995). Development of a Global Aging System Short and Long Term Aging of Asphalt Cements. *J. Assoc. Asphalt Paving Technol.* 64:393-430.

Petersen, J. C., Plancher, H., and Miyake, G. (1983). Chemical Reactivity and Flow Properties of Asphalts Modified by Metal Complex-Induced Reaction with Atmospheric Oxygen. *Proc. Assoc. Asphalt Paving Technol.* 52:32-60.

Petersen, J. C. and Harnsberger, P. M. (1998). Asphalt Aging: Dual Oxidation Mechanism and Its Interrelationships with Asphalt Composition and Oxidative Age Hardening. *Transp. Res. Rec.* 1638:47-55.

Petersen, J. C. (2009). *A Review of the Fundamentals of Asphalt Oxidation Chemical, Physicochemical, Physical Property, and Durability Relationships.* Transportation Research Circular, E-C140. Washington D.C.: Transportation Research Board.

Pfeiffer, J. P. (1950). *The Properties of Asphaltic Bitumen*. Elsevier, Amsterdam.

Prapaitrakul, N., Han, R., Jin, X., and Glover, C. J. (2009). A Transport Model of Asphalt Binder Oxidation in Pavements. *Road Mater. Pavement Des*. 10/SI:95-113.

R Development Core Team. (2011). *R: A Language and Enviroment for Statistical Computing.* Vienna, Austria: R Foundation for Statistical Computing.

Ruan, Y., Davison, R. R., and Glover, C. J. (2003). An Investigation of Asphalt Durability: Relationships between Ductility and Rheological Properties for Unmodified Asphalts. *Pet. Sci. Technol.* 21:231-254.

Van Gooswilligen, G., Berger H., and De Bats, F. Th. (1985). Oxidation of Bitumens in Various Tests. *Third Eurobitumen Symposium.* 95–101. The Hague, Netherlands.

Van Oort, W. P. (1956). Durability of Asphalt. *Ind. Eng. Chem.* 48:1196-1201.

Walubita, L. F., Martin, A. E., Glover, C. J., Jung, S. H., Cleveland, G. S., Lytton, R. L., Park, E. S. (2006). Application of the Calibrated Mechanistic Approach with Surface Engergy (CMSE) Measurements for Fatigue Characterization of Asphalt Mixtures (With Discussion). *J. Assoc. Asphalt Paving Technol.* 75:457-489.

Willams, R. C., and McCready, N. S. (2008). *The Utilization of Agriculturally Derived Lignin as an Antioxidant in Asphalt Binder*. Final Report No. 06-260. Iowa: Center for Transportation Research and Education.

APPENDIX A

CA GROWTH OF BINDER: DATA VERSUS MODEL CALCULATIONS

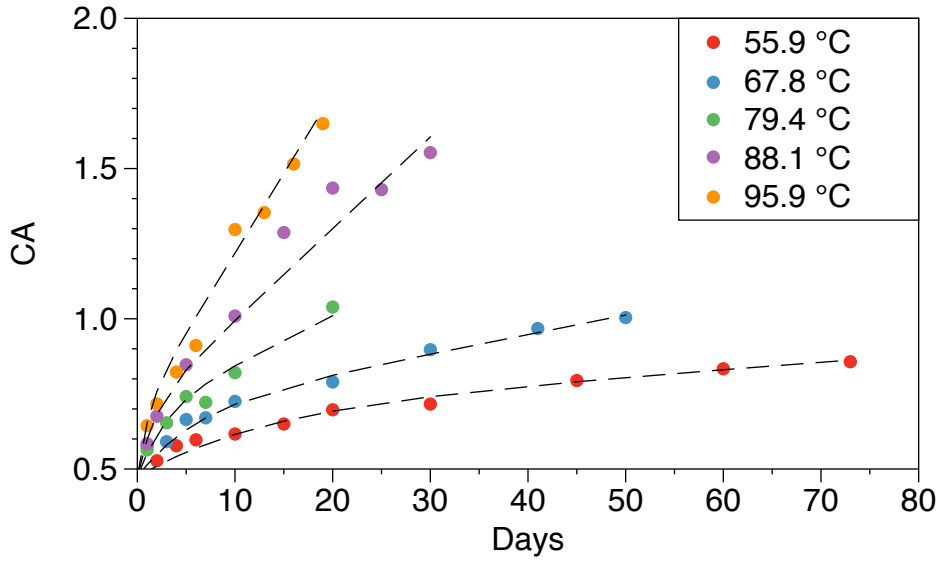

Figure A.1. CA growth of Alon PG70-22 at five temperatures in air. (Data: Symbols, Model Calculations: Dashed Lines)

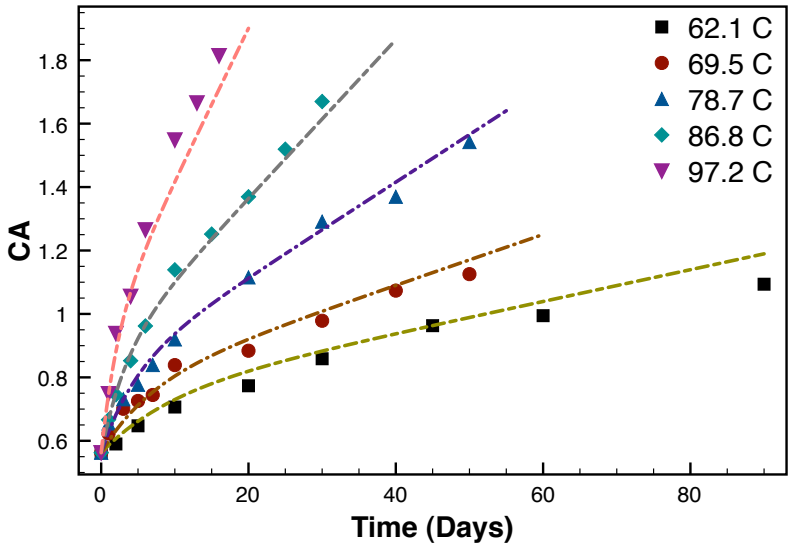

Figure A.2. CA growth of Alon PG76-22 at five temperatures in air. (Data: Symbols, Model Calculations: Dashed Lines)

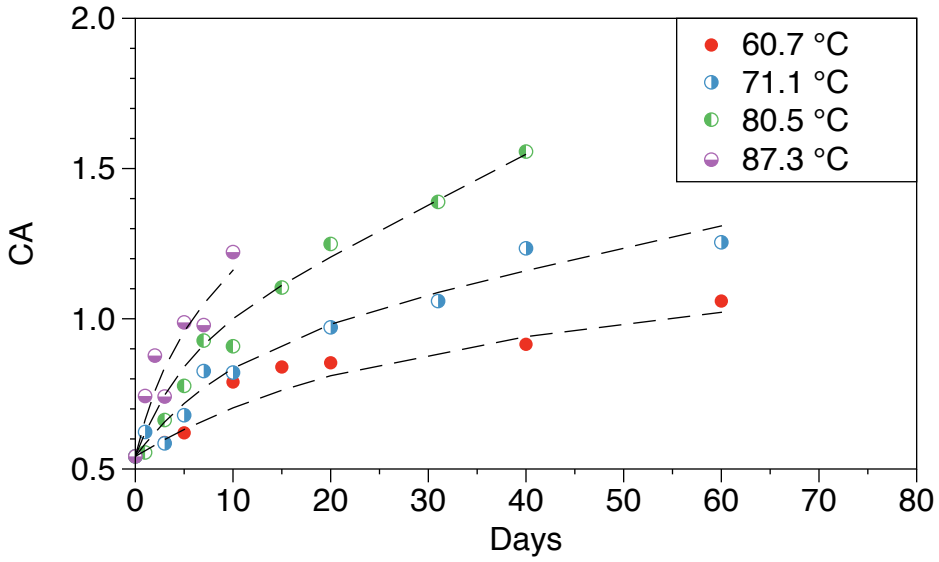

Figure A.3. CA growth of Lion PG64-22 at four temperatures in air. (Data: Symbols, Model Calculations: Dashed Lines)

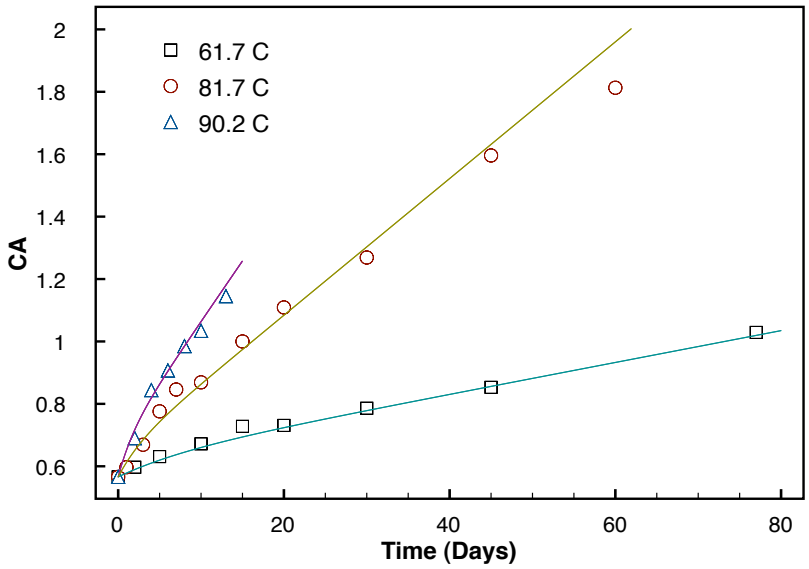

Figure A.4. CA growth of Martin PG64-22 at three temperatures in air. (Data: Symbols, Model Calculations: Dashed Lines)

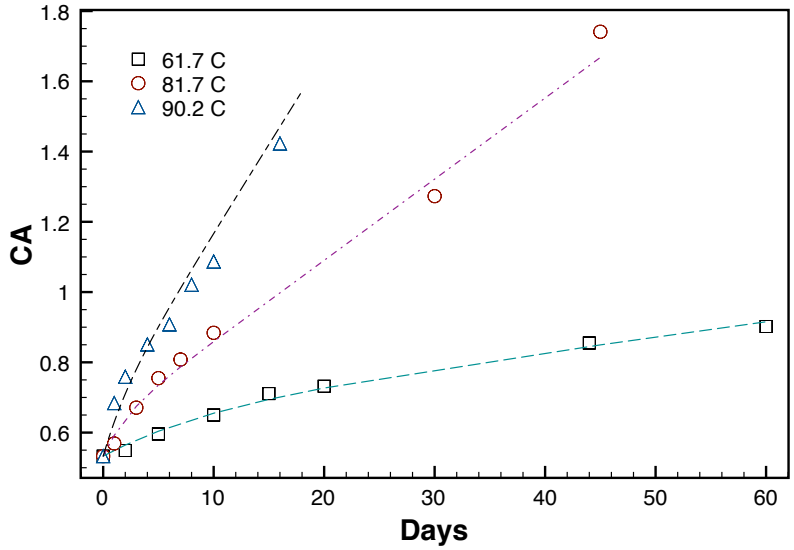

Figure A.5. CA growth of Martin PG70-22 at three temperatures in air. (Data: Symbols, Model Calculations: Dashed Lines)

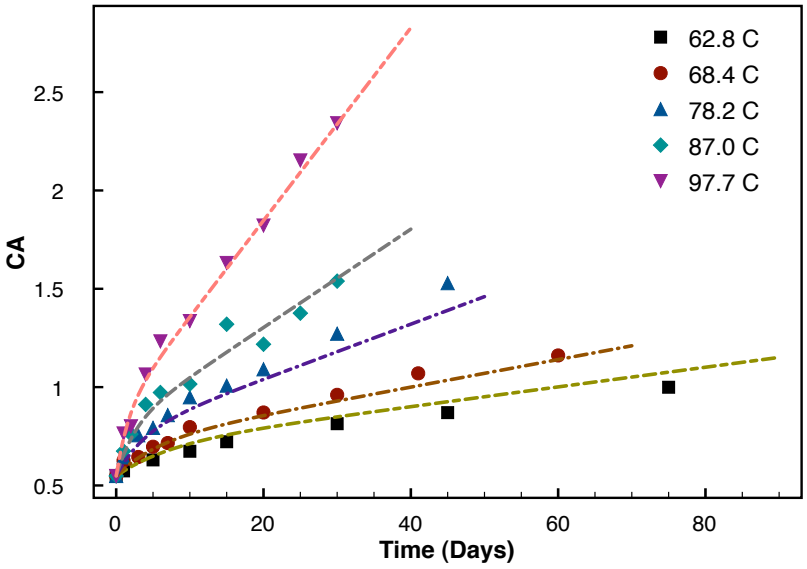

Figure A.6. CA growth of SEM PG64-22 at five temperatures in air. (Data: Symbols, Model Calculations: Dashed Lines)

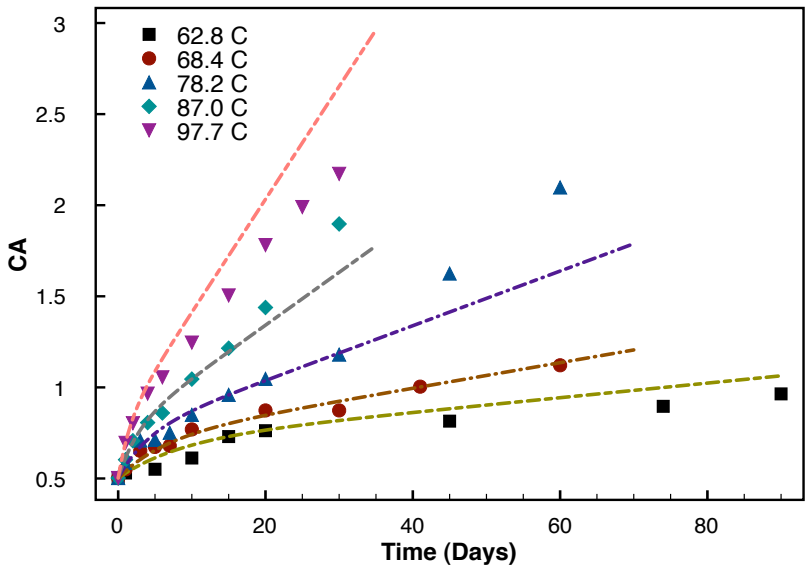

Figure A.7. CA growth of SEM PG70-22 at five temperatures in air. (Data: Symbols, Model Calculations: Dashed Lines)

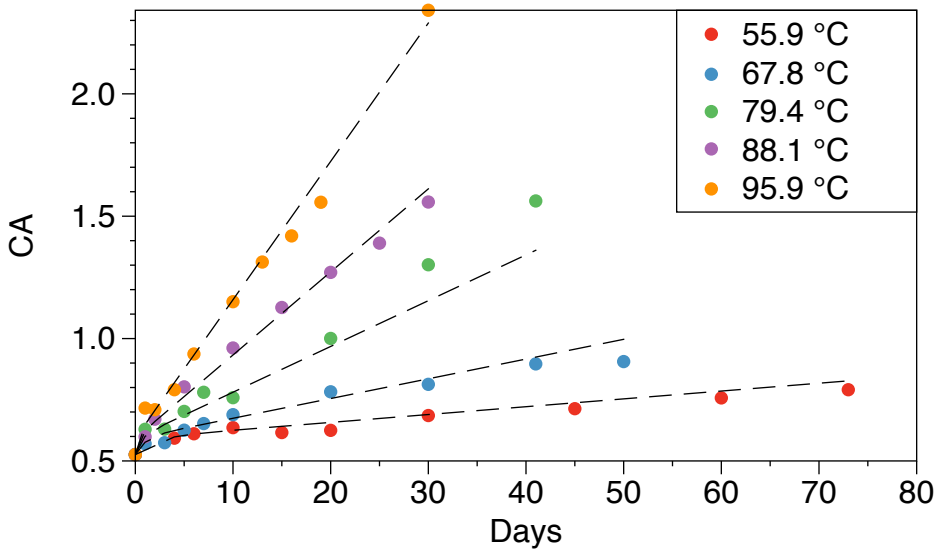

Figure A.8. CA growth of SEM PG70-28 at five temperatures in air. (Data: Symbols, Model Calculations: Dashed Lines)

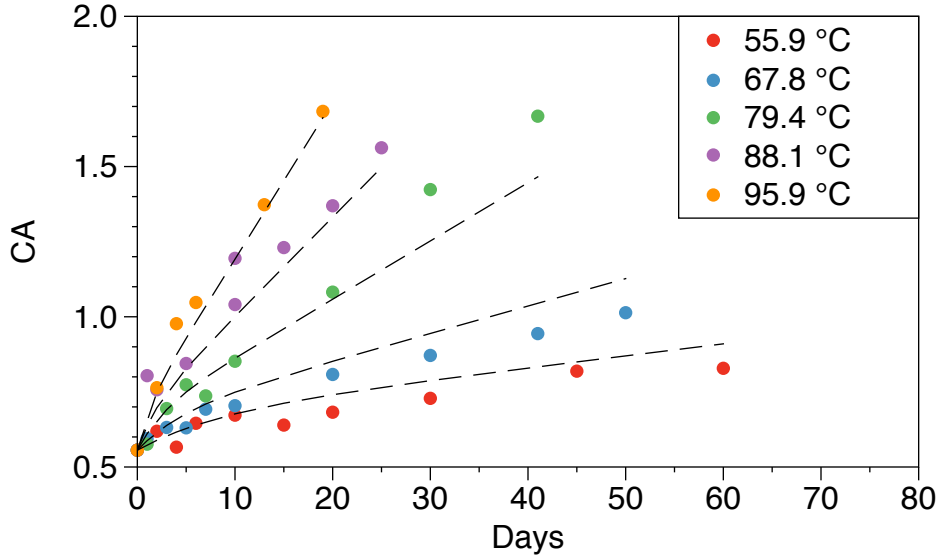

Figure A.9. CA growth of SEM PG76-22 at five temperatures in air. (Data: Symbols, Model Calculations: Dashed Lines)

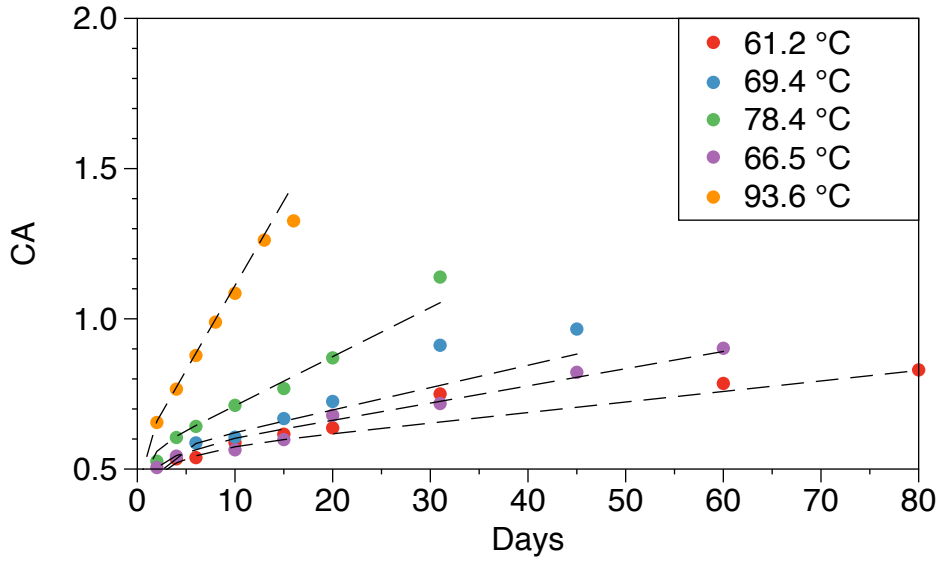

Figure A.10. CA growth of Valero-C PG64-22 at five temperatures in air. (Data: Symbols, Model Calculations: Dashed Lines)

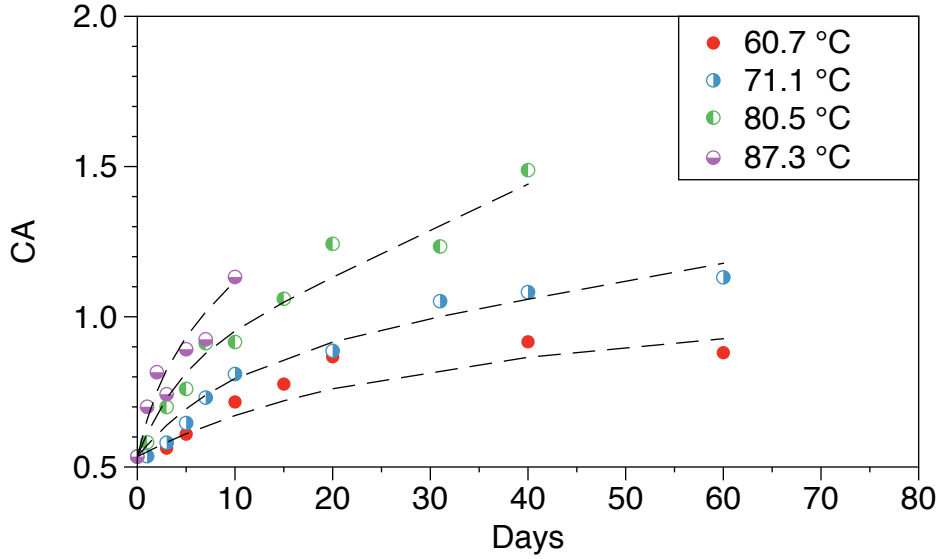

Figure A.11. CA growth of Valero-C PG70-22 at four temperatures in air. (Data: Symbols, Model Calculations: Dashed Lines)

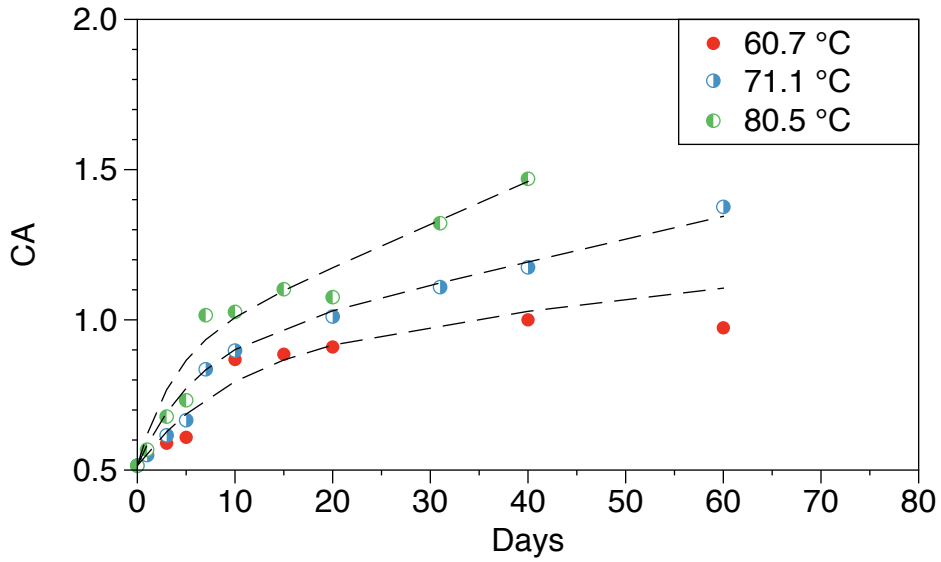

Figure A.12. CA growth of Valero-C PG76-22 at three temperatures in air. (Data: Symbols, Model Calculations: Dashed Lines)

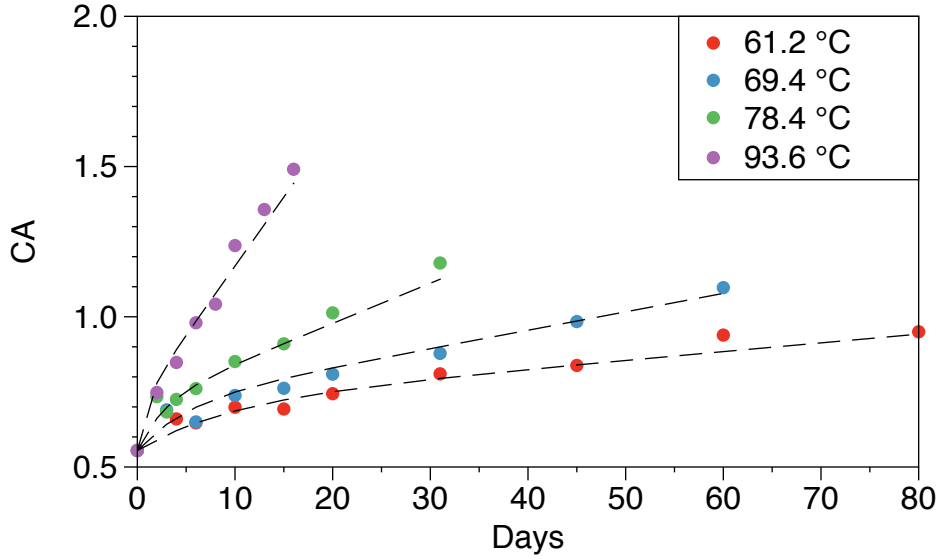

Figure A.13. CA growth of Valero-H PG76-22 at four temperatures in air. (Data: Symbols, Model Calculations: Dashed Lines)

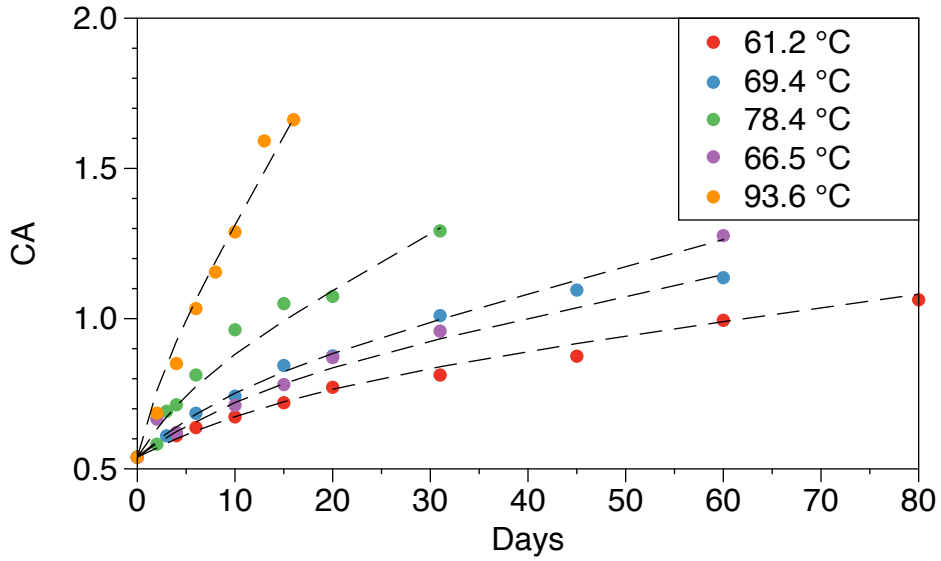

Figure A.14. CA growth of Valero-O PG64-22 at five temperatures in air. (Data: Symbols, Model Calculations: Dashed Lines)

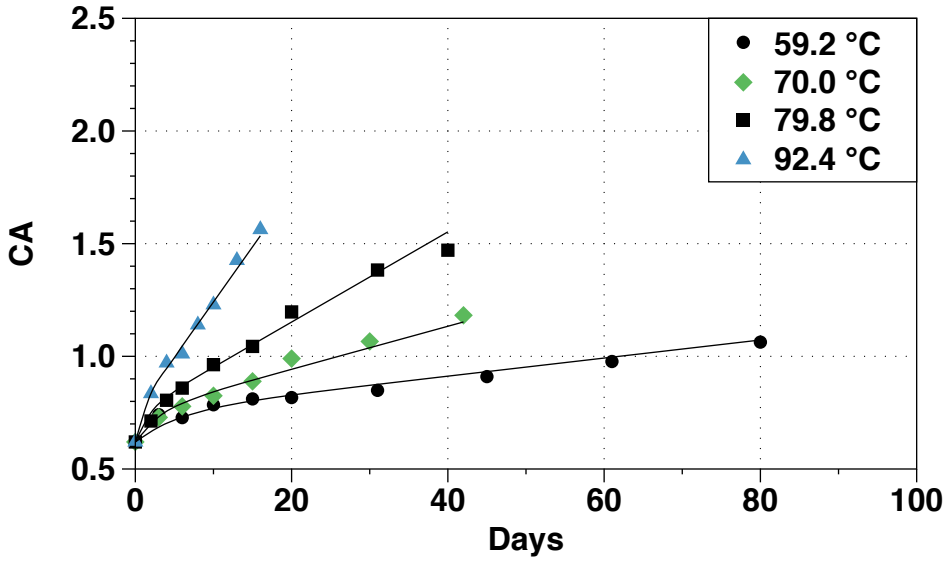

Figure A.15. CA growth of NuStar PG67-22 at four temperatures in air. (Data: Symbols, Model Calculations: Solid Lines)

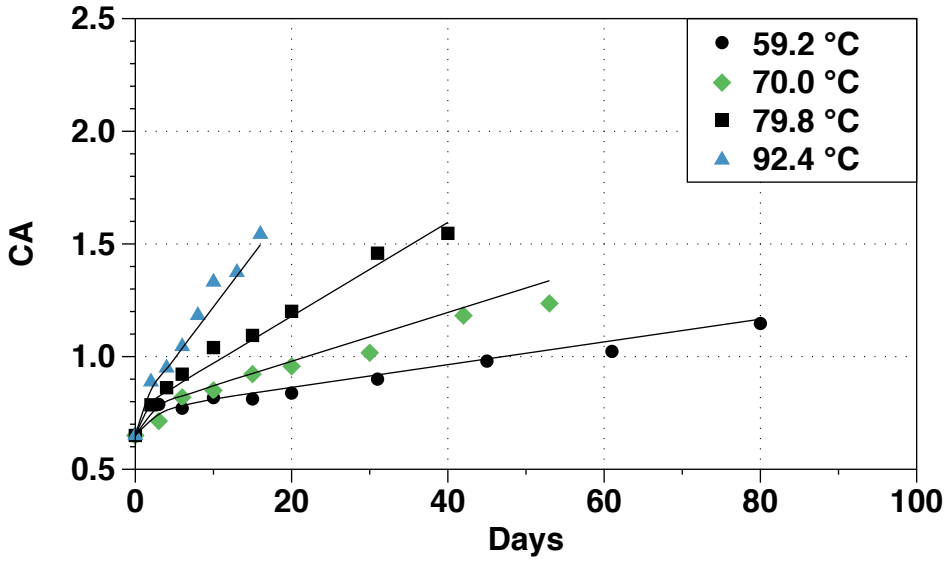

Figure A.16. CA growth of NuStar PG76-22 at four temperatures in air. (Data: Symbols, Model Calculations: Solid Lines)

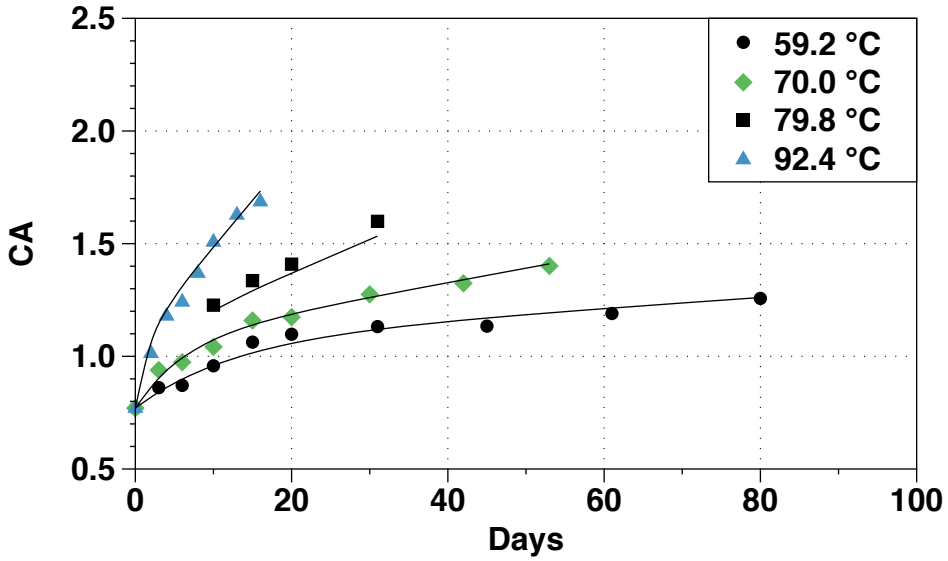

Figure A.17. CA growth of Valero-B PG64-16 at four temperatures in air. (Data: Symbols, Model Calculations: Solid Lines)

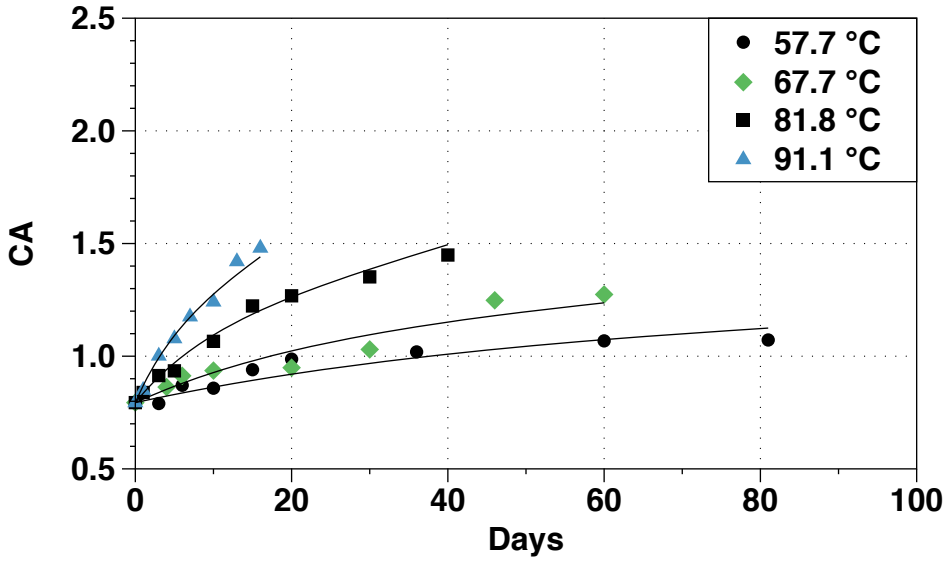

Figure A.18. CA growth of AAD-1 at four temperatures in air. (Data: Symbols, Model Calculations: Solid Lines)

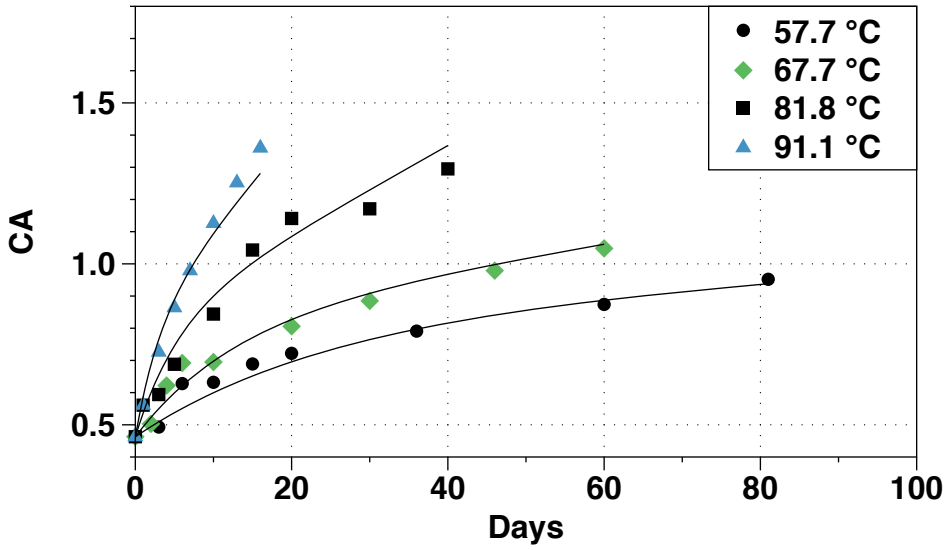

Figure A.19. CA growth of AAM-1 at five temperatures in air. (Data: Symbols, Model Calculations: Solid Lines)

APPENDIX B

HARDENING SUSCEPTIBILITY OF BINDER LOW SHEAR RATE LIMITING VISCOSITY

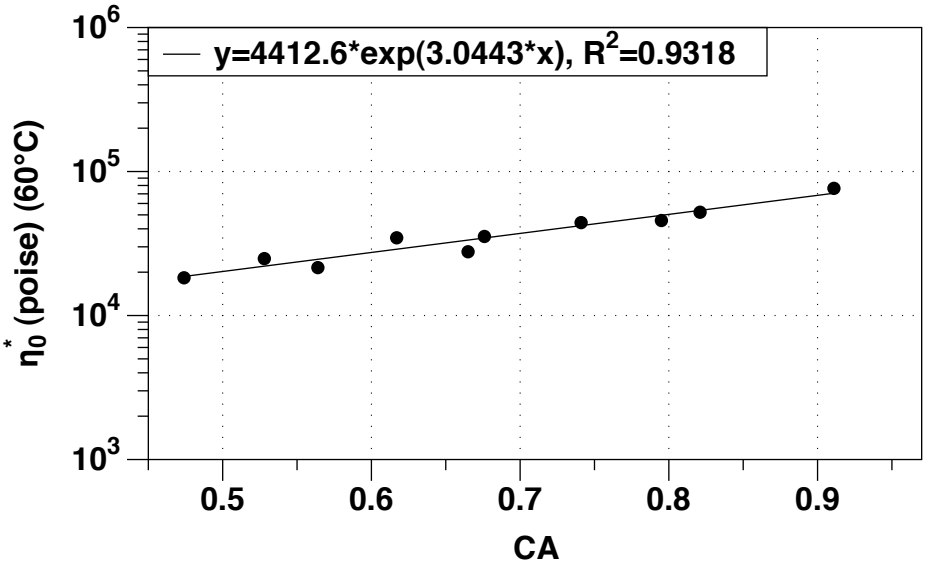

Figure B.1. HS of limiting viscosity of Alon PG70-22.

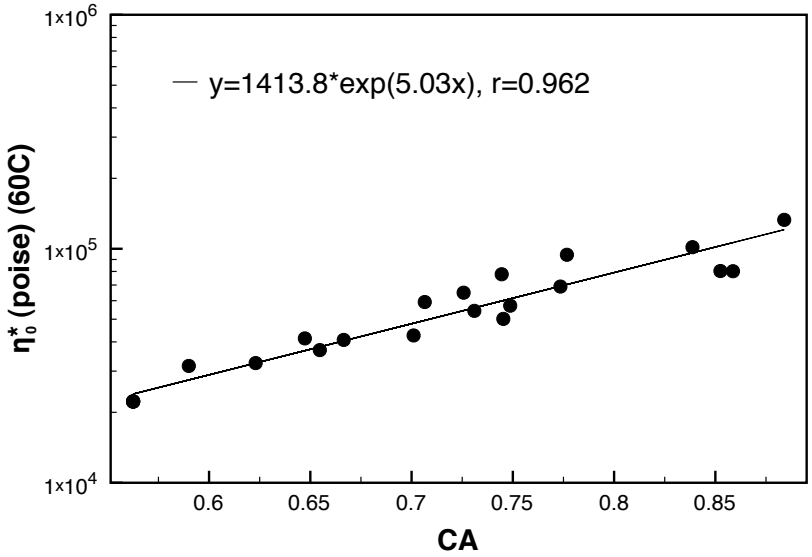

Figure B.2. HS of limiting viscosity of Alon PG76-22.

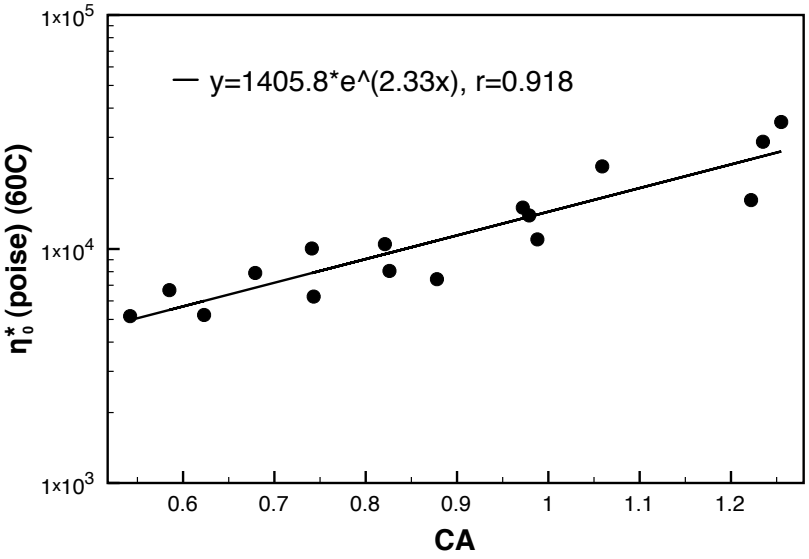

Figure B.3. HS of limiting viscosity of Lion PG64-22.

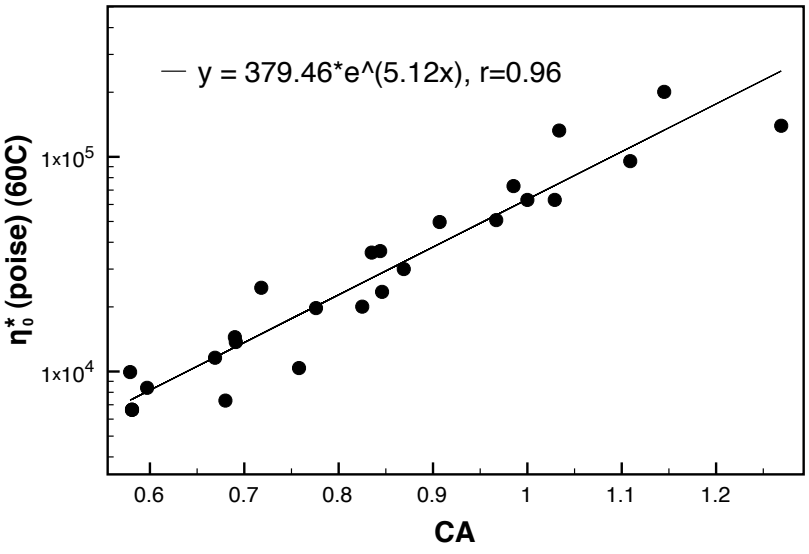

Figure B.4. HS of limiting viscosity of MARTIN PG64-22.

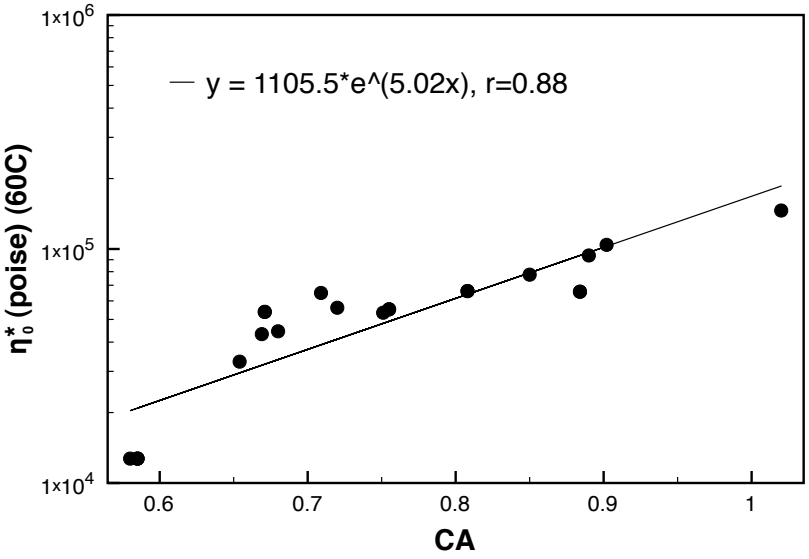

Figure B.5. HS of limiting viscosity of MARTIN PG70-22.

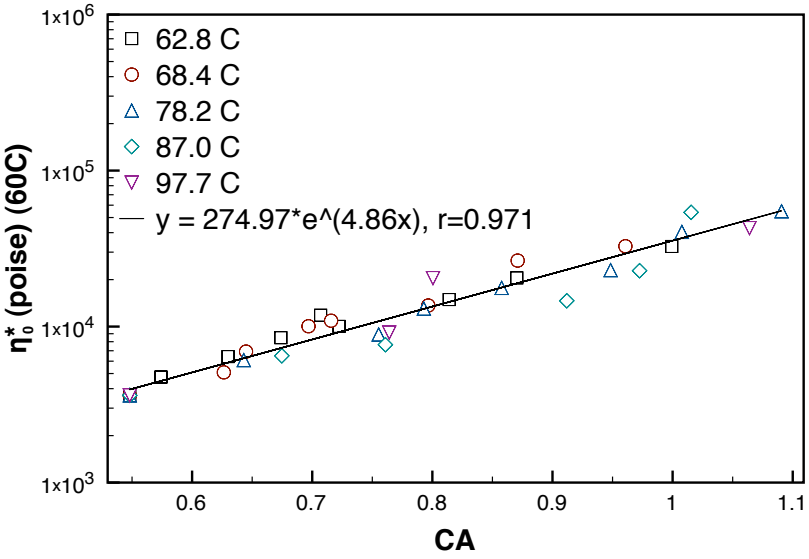

Figure B.6. HS of limiting viscosity of SEM PG64-22.

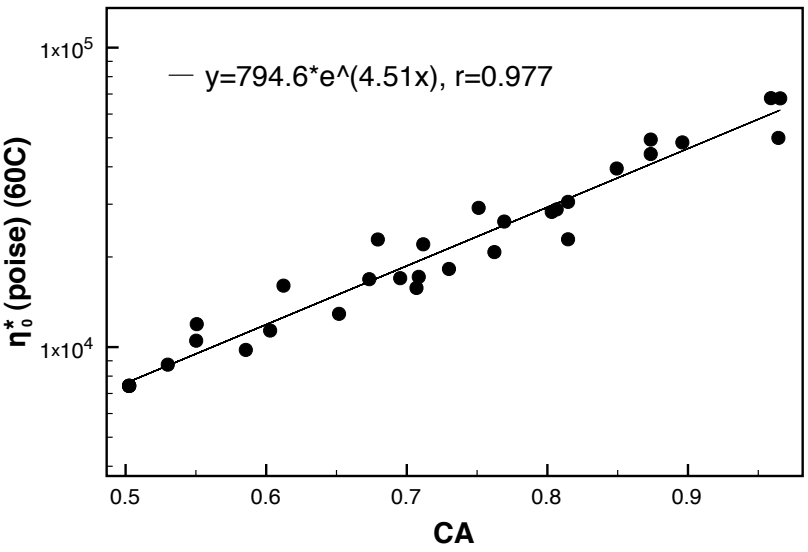

Figure B.7. HS of limiting viscosity of SEM PG70-22.

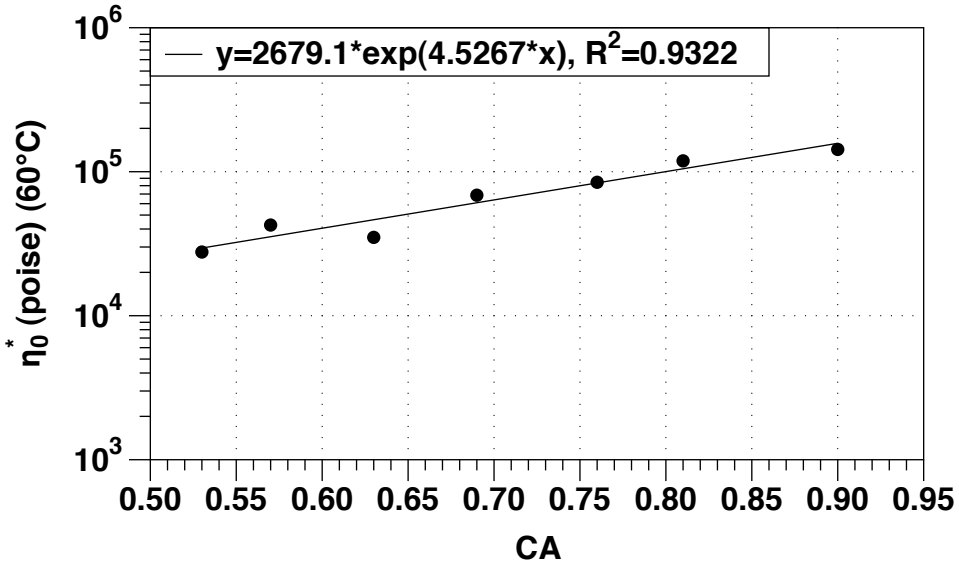

Figure B.8. HS of limiting viscosity of SEM PG70-28.

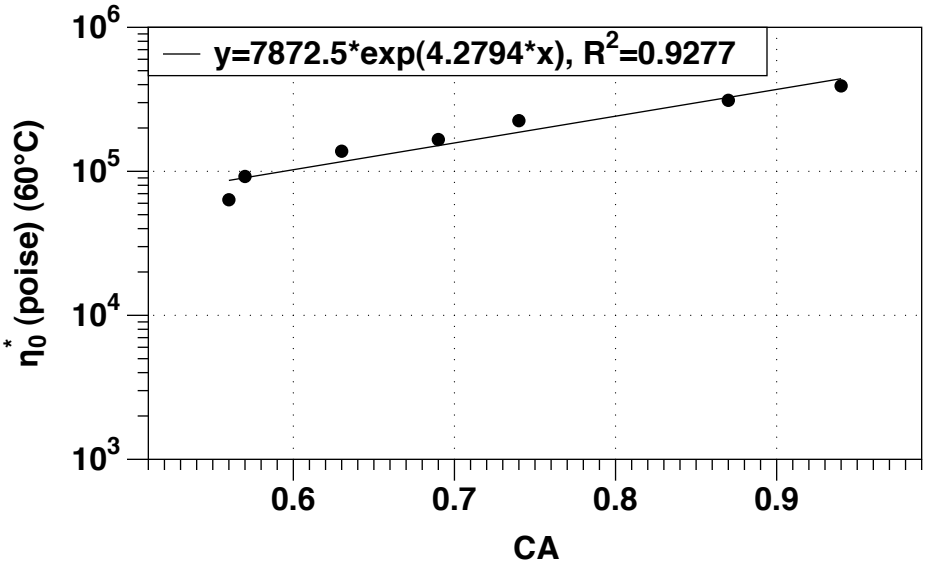

Figure B.9. HS of limiting viscosity of SEM PG76-22.

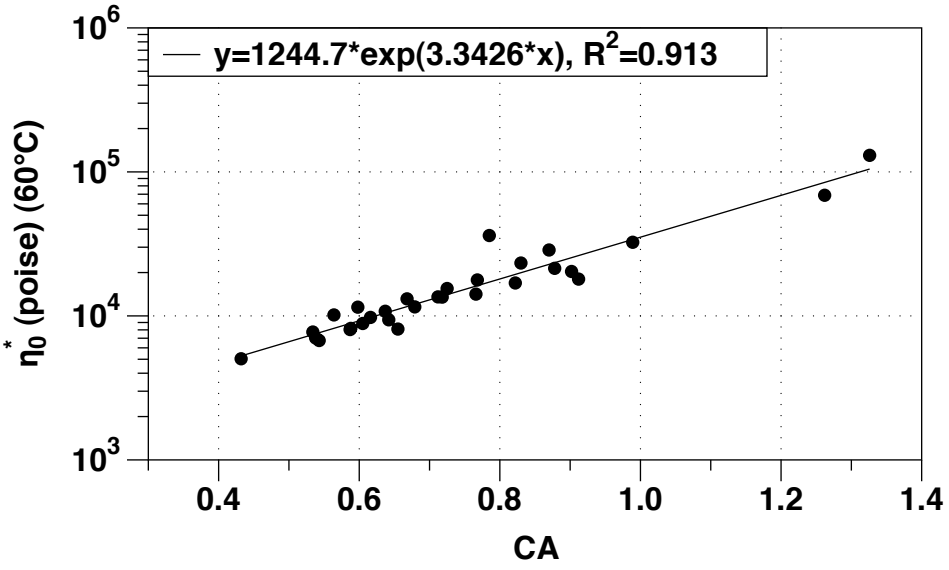

Figure B.10. HS of limiting viscosity of VAL-C PG64-22.

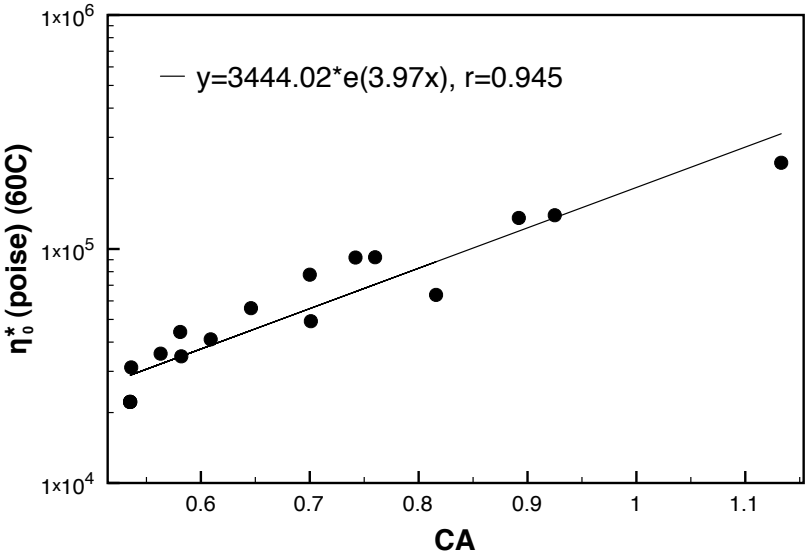

Figure B.11. HS of limiting viscosity of VAL-C PG70-22.

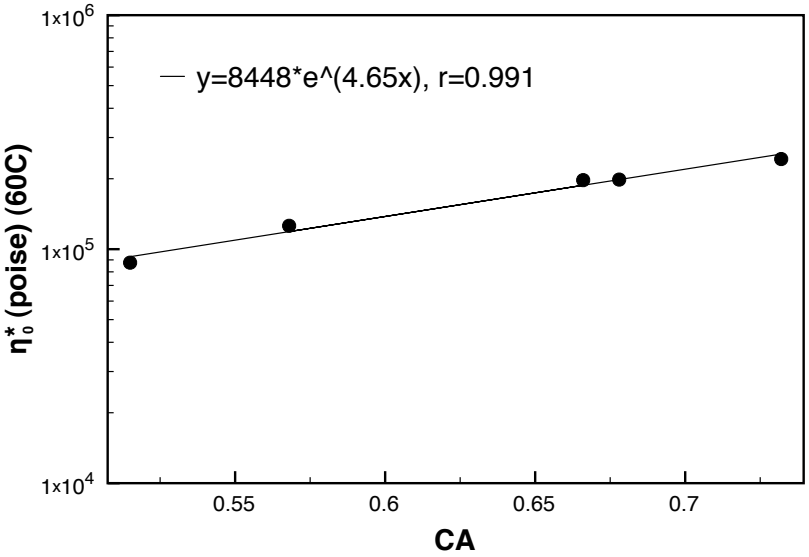

Figure B.12. HS of limiting viscosity of VAL-C PG76-22.

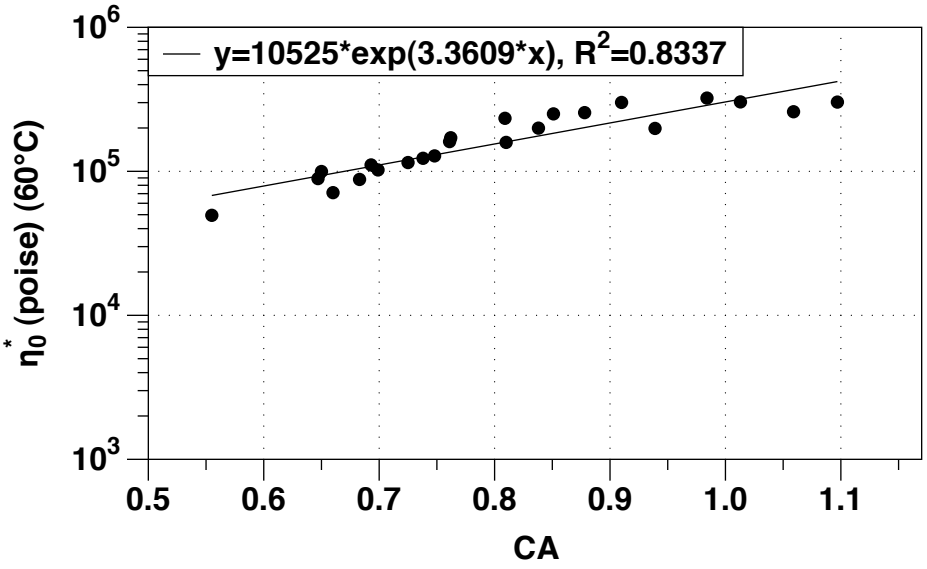

Figure B.13. HS of limiting viscosity of VAL-H PG76-22.

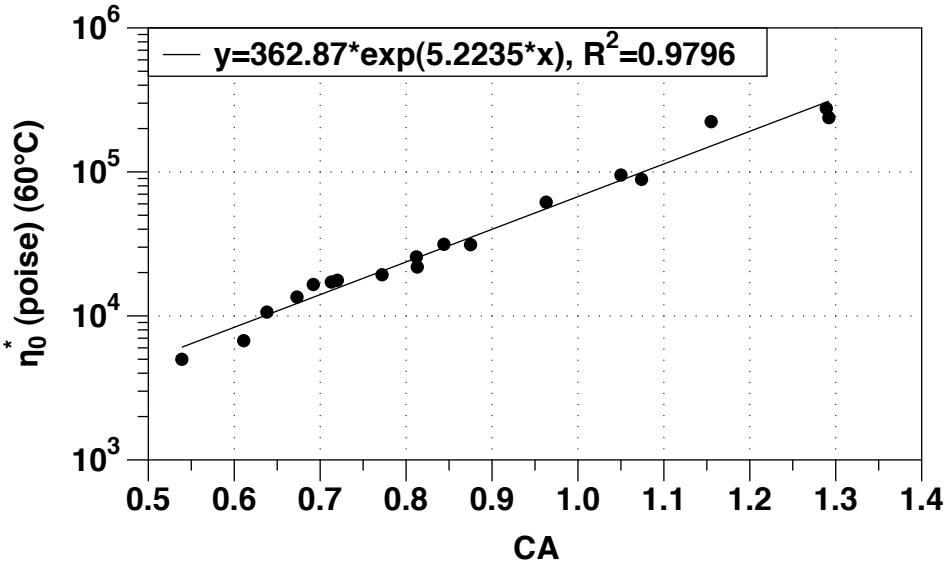

Figure B.14. HS of limiting viscosity of VAL-O PG64-22.

VITA

Name: Xin Jin

Address: Department of Chemical Engineering, c/o Dr. Charles Glover
Texas A&M University College Station, TX 77843-3122

Email Address: jinxinhd@yahoo.cn

Education: B.E., Automation, Zhejiang University, 2005
M.S., Chemical Engineering, Texas A&M University, 2009